THE PENETRATION AND MIXING OF A SONIC HYDROGEN JET INJECTED NORMAL TO A MACH 4 AIRSTREAM

By

Ruben Clayton Rogers

Thesis submitted to the Graduate Faculty of the

Virginia Polytechnic Institute

in candidacy for the degree of

MASTER OF SCIENCE

in

Aerospace Engineering

March 1970

THE PENETRATION AND MIXING OF A SONIC HYDROGEN JET INJECTED NORMAL TO A MACH 4 AIRSTREAM

By

Ruben Clayton Rogers

ABSTRACT

An investigation has been conducted to determine the effects of jet-to-free-stream dynamic pressure ratio on the penetration and mixing of a sonic hydrogen jet injected normal to a Mach 4 airstream. The hydrogen gas was injected from a circular nozzle flush mounted in a flat plate with a turbulent boundary-layer thickness of 2.70 injector exit diameters at the injector station. The investigation was conducted for values of the dynamic pressure ratio ranging from 0.5 to 1.5. At five downstream stations between 7 and 200 injector diameters the mixing region was surveyed to obtain hydrogen volume concentration and pressure profiles.

Results of the investigation indicate that the thick boundary layer had significant effects on the penetration and maximum concentration trajectories when compared to data correlations from other sources. The penetration trajectory was found to be proportional to the dynamic pressure ratio raised to the 0.3 power. The decay of the maximum concentration was very rapid in the near field and inversely proportional to $(x/d_j)^{0.8}$ at downstream distances greater than 30 jet diameters.

THE PENETRATION AND MIXING OF A SONIC HYDROGEN JET INJECTED NORMAL TO A MACH 4 AIRSTREAM

by

Ruben Clayton Rogers

Thesis submitted to the Graduate Faculty of the
Virginia Polytechnic Institute
in partial fulfillment of the requirements for the degree of

MASTER OF SCIENCE

in

Aerospace Engineering

APPROVED: Fred R. DeJarnette
Chairman, Dr. Fred R. DeJarnette

Joseph A. Schetz
Dr. Joseph A. Schetz

W. P. Harrison, Jr.
Prof. W. P. Harrison, Jr.

March 1970

Blacksburg, Virginia

II. TABLE OF CONTENTS

At a particular value of x/d the maximum concentration was proportional to $q_r^{1/2}$. Nondimensional concentration profiles, represented by Gaussian-type functions, on the vertical centerline showed similarity at values of x/d equal to or greater than 60.

III. ACKNOWLEDGMENTS

The author wishes to express thanks to the National Aeronautics and Space Administration for the use of research facilities at the Langley Research Center in acquiring the data presented in this thesis. Appreciation is also expressed to Dr. Fred R. DeJarnette of the Aerospace Engineering Department of the Virginia Polytechnic Institute for his advice and assistance, and to Mr. John R. Henry of the Langley Research Center for his technical comments and suggestions concerning the analysis of the data. A special thanks to Mrs. Pat Reagon for her aid in the preparation of the figures, and to Mrs. Marge Mills for typing the first draft of the text.

IV. LIST OF FIGURES

FIGURE PAGE

V. INTRODUCTION

Recent projects of the National Aeronautics and Space Administration have been concerned with the design and development of research engines for operation in the Mach 4 to Mach 8 flight regime (ref. 1). The engine is an axisymmetric hydrogen-fueled ramjet and employs supersonic combustion at flight speeds above Mach 6. Advanced hypersonic vehicles, such as a reusable launch vehicle with an airbreathing propulsion system for the first stage, are currently under investigation (ref. 2). The propulsion system will be a supersonic combustion ramjet with operation up to Mach 12. A flight Mach number of 12 corresponds to a combustor-entrance Mach number of 4. Preliminary designs indicate that with the length of the inlet and compression surfaces required at these high flight Mach numbers, a significant portion of the flow entering the combustor will consist of a boundary layer. The accurate analysis and design of a supersonic combustor requires a knowledge of the fuel-air mixing characteristics. In addition, injecting the fuel in a way that provides for a nearly uniform fuel distribution and a short mixing length without producing significant thrust penalties is desirable. Parallel or coaxial injection, while contributing significantly to the thrust, requires a longer mixing length and has less penetration than does injection perpendicular to the airstream (refs. 3 and 4).

Normal sonic injection of various gases and gaseous mixtures issuing from a discrete circular hole in a flat plate into a supersonic airstream has been investigated and reported in references 4 to 9 inclusive. These data are generally for conditions corresponding to high values of jet-to-free-stream dynamic pressure ratio. Unpublished data available at the Langley Research Center indicate that the shortest mixing length is obtained at the lowest value of jet-to-free-stream dynamic pressure ratio at which the injector operates choked. Analytical methods for predicting the initial penetration of the jet and the jet trajectory in the unconfined supersonic main-stream have been developed from empirical or semi-empirical data correlations (see refs. 7 to 9). Generally, any effect of the molecular weight of the injected gas or the main-stream boundary-layer thickness has not been considered. For application to the design of a supersonic combustor, the primary interest is in the far-field mixing region rather than the complex flow in the vicinity of the injector.

The present investigation was conducted to provide information about the effect of jet-to-free-stream dynamic pressure ratio and a thick boundary layer on the mixing of hydrogen injected normal to a uniform supersonic airstream. These data are needed to aid in constructing analytical methods that yield reliable predictions about the mixing process in supersonic combustors. Hydrogen gas was injected from a 0.1016-centimeter-diameter sonic nozzle perpendicular to the surface of a flat plate mounted in the 23-centimeter-square tunnel test section. The tests were conducted at a free-stream Mach number of 4.03, stagnation temperature of 300° K, stagnation pressures of 13.6 and 20.4 atmospheres, giving Reynolds numbers per meter of 6.19×10^7 and

9.28×10^7, respectively. Boundary-layer thickness on the flat plate at the injector station was approximately 2.70 injector diameters. Jet conditions were such that ratios of jet-to-free-stream momentum flux of 0.5, 0.75, 1.0, and 1.5 were obtained. Measurements of hydrogen volume concentration, pitot pressure, and static pressure were obtained by vertical and horizontal surveys of the flow field at downstream stations of 7, 30, 60, 120, and 200 injector diameters.

VI. LIST OF SYMBOLS

A	streamtube cross-section area, meter^2
b_1	exponent defined in equation (9)
b_2	exponent defined in equation (10)
C_D	drag coefficient
d	injector nozzle exit diameter, meter
d_j	equivalent jet exit diameter = $dK^{1/2}$
f	fuel-air mass ratio
K	injector nozzle discharge coefficient
$\dot{m}$	mass flow rate, kilogram/second
M	Mach number
p	absolute pressure, Newton/meter^2 or atm
p_b	effective back pressure, Newton/meter^2
q_r	ratio of jet-to-free-stream dynamic pressure = $(\rho V^2)_j/(\rho V^2)_\infty$
Re	Reynolds number
h	distance measured along centerline of emerging jet, meter
T	absolute temperature, °Kelvin
V	velocity, meter/second
x	longitudinal coordinate
y	lateral coordinate
z	vertical coordinate
α	hydrogen mass fraction
β	air mass flux parameter = $(\rho V)_x(1 - \alpha)$ kilogram/meter^2-second
δ	boundary-layer thickness, meter

δ^*	boundary-layer displacement thickness, meter
ν	hydrogen volume fraction
ξ	hydrogen mass flow rate parameter $\equiv \alpha(\rho V)_x/(\rho V)_j$
θ	slope of emerging jet centerline measured from horizontal, degree
ρ	mass density, kilogram/meter^3

Subscripts:

∞	free-stream conditions
0	conditions at the edge of the mixing region where $\nu = 0.005$
1	conditions in undisturbed flow upstream of injector
5	conditions at which the mass concentration is half maximum
j	jet conditions
t	stagnation conditions
x	survey point
max	maximum value
ref	reference value
α	conditions at which concentration is maximum

Superscripts:

$\overline{(\ )}$	average quantity
$(\ )'$	conditions behind normal shock

VII. MODEL AND FACILITY

Test Apparatus and Model

A sketch of the stainless steel rectangular flat plate used in the experiments is shown in figure 1. The plate leading edge was a 2° wedge tapering to a cylindrical leading edge of approximately 0.0127 centimeter thickness, followed by a 10° wedge. A 0.1016-centimeter-diameter sonic nozzle was flush mounted perpendicular to the plate surface 18.6 centimeters from the plate leading edge. Details of the nozzle are shown inset in figure 1. The injector tube had a constant area section approximately three exit diameters long and was fed by a section of tube 4 centimeters long and 0.1524 centimeters inside diameter that acted as a plenum. The plenum section was fed by a 0.476-centimeter-diameter tube in which the jet total pressure was measured. For sonic operation of the injector, the Mach number in the plenum section is approximately 0.30 and would probably be fully developed pipe flow. Because of the rapid acceleration, the flow in the injector tube would be only slightly affected by the boundary layer in the supply tube and would not be fully developed pipe flow.

The tests were conducted in a continuous flow supersonic tunnel with the flat plate spanning the 23-centimeter by 23-centimeter test section. The top surface of the plate was positioned horizontally along the longitudinal centerline of the tunnel test section. The tunnel exhausted to atmosphere and had a two-dimensional fixed geometry nozzle and a second minimum followed by a subsonic diffuser. The test section Mach number above the boundary layer at the injection station was 4.03 (ref. 4). Tests were conducted at stagnation temperatures of 300° K, stagnation pressures of 13.6 and 20.4 atmospheres, giving corresponding unit Reynolds numbers of 6.19×10^7 and 9.28×10^7 per meter. Boundary-layer surveys were made at the injector exit station at both of the tunnel stagnation pressures. Profiles of total pressure and velocity for both cases are presented in figure 2. The boundary-layer thickness was taken as the point at which the velocity reached 99 percent of free stream with values of 2.70 injector exit diameters obtained at both free-stream stagnation pressures. Also presented in figure 2 are theoretical results obtained from a computer program reported in reference 10. The theoretical results were obtained for conditions corresponding to a free-stream total pressure of 20.4 atmospheres and agreed well with the data.

Secondary flow.- The routing of the hydrogen gas within the test cell is presented schematically in figure 3. Hydrogen gas was stored in trailers and supplied to the test cell by a 7.62-centimeter-diameter line equipped with pressure-controlled valves and a nitrogen purge system. An electrically controlled, air-operated three-way ball valve was used to shut off hydrogen flow inside the test cell and to vent the supply line within the building to the atmosphere. Hydrogen flow rate was measured by a 0.3175-centimeter-diameter sharp-edged corner tap orifice meter. Upstream pressure at the orifice meter was set and maintained by an air-controlled pressure-regulated valve and the orifice pressure drop and hydrogen jet total pressure controlled by an air-operated valve immediately downstream of the flow meter. Hydrogen total temperature was measured with a standard iron-constantan thermocouple inserted in a filter positioned between the orifice meter and injector. Jet total pressure was measured near the injector exit by mounting a 0.1016-centimeter outside-diameter tube in the 0.476 centimeter-diameter injector supply tube. Calculations indicated that the measured pressure would be within 99 percent of the jet total pressure. The apparatus was operated over a jet total pressure range of 2 to 4 atmospheres corresponding to jet-to-free-stream dynamic pressure ratios of 0.5 to 1.5. The exact test conditions are presented in the following table.

Test condition	q_r	$p_{t,\infty}$ (atm)	$p_{t,j}$ (atm)	$\dot{m}_{H_2}$ (gm/sec)	Re (m^{-1})	δ/d
1	0.50	20.4	1.986	0.0820	9.28×10^7	2.70
2	0.75	20.4	2.980	0.1230	9.28×10^7	2.70
3	1.00	13.6	2.647	0.1094	6.19×10^7	2.70
4	1.50	13.6	3.960	0.1641	6.19×10^7	2.70

Chromatograph system.- A tube attached to the injector nozzle supply line supplied 100 percent hydrogen samples for full-scale chromatograph readings. The sample collection and analysis system is shown in figure 3. During a survey gas samples of the hydrogen-air mixture were taken through a pitot probe with the aid of a vacuum pump at mass flow rates as high as 4.17×10^{-3} gm/sec. The sample flow to the chromatograph was metered to 5.56×10^{-5} gm/sec by an electrically controlled microvalve and the remaining flow bypassed and exhausted into the test cell. Both the sample and bypassed mass flow rates were measured by thermoconductivity flow meters. A nitrogen bottle was used to insure complete purging of the gas collection and analysis system.

Instrumentation

Gas analyzer.- The volumetric concentration of hydrogen in the gas samples was measured by a process gas chromatograph. The sample gas and a carrier gas (nitrogen) flow continuously through the chromatograph. At the beginning of a 1-minute cycle a portion of the sample gas is isolated and forced by the carrier gas through a molecular sieve and a column consisting of a length of stainless steel tubing packed with silica gel. This provides a qualitative identification of each component since each will process through the column at a predictable rate. The quantity of each component is determined by four thermoconductivity detectors of which two are always exposed to the carrier gas. The unbalance of the detector bridge provides a voltage output proportional to the cooling effect, and hence, is a measure of the concentration of the separated sample components relative to the carrier gas. The voltage output is recorded by a pen deflection on a strip chart. Readout controls were adjusted so that only the hydrogen concentration was detected. The pen deflection for 100 percent hydrogen taken from the supply line was recorded before each survey, and the repeatability of the instrument checked to a variation of less than 1/2 percent full scale. This corresponds to an error in hydrogen volume fraction of ±0.005. Further information about gas chromatography may be found in references 11 and 12. The gas analyzer was calibrated with known mixtures of hydrogen and air. The calibration points and an equation for a curve through the points are presented in figure 4. During the course of the tests, the calibration was kept up to date by spot-check calibrations, using hydrogen-nitrogen mixtures of known concentration.

Probe description.- The gas-sampling pitot probe and the static probe are shown in figure 5. The pitot-sampling probe is a boundary-layer survey type with the probe tip mounted in a 7.94-millimeter-diameter supporting tube offset to allow for actuator rod clearance. The actuator mechanism provided for probe movement for vertical traversing and yaw in the horizontal plane. A variable resistance pot electrically coupled to a counter indicated the probe position. The counter was calibrated with a precision dial gauge and gave the probe position with an accuracy of ±0.127 millimeter in the traverse mode and ±0.10° in the yaw mode. The static pressure probe was of similar design and had a 28° cone angle and four 0.203-millimeter orifices located at 14 probe diameters from the tip.

Flow measurement.- The injected gas was measured with a 0.3175 centimeter-diameter sharp-edged corner tap orifice meter as shown in figure 3. Orifice meter upstream static pressure and pressure drop were measured by a 1.379×10^6 N/m^2 transducer and a 6.895×10^3 N/m^2 differential pressure transducer, respectively. The static temperature at the meter was assumed to be the same as the jet stagnation temperature. Hydrogen mass flow rate through the orifice meter was calculated from an equation derived from a hydrogen corrected air calibration of the orifice meter. The sample flow rate to the chromatograph and the bypass flow rate were measured by thermoconductivity mass flow rate meters with ranges of 0 to 100 sccm (1.39×10^{-4} gm/sec) and 0 to 3,000 sccm (4.17×10^{-3} gm/sec), respectively. The discharge coefficient of the injector nozzle, based on orifice meter measurements, normally ranged from 0.73 to 0.78, with an average value of 0.76. In some instances, values of K as low as 0.69 were obtained; calculations indicate that a film of dirt on the order of 0.025 millimeter thick could have caused this low value.

Pitot pressure was measured with a 3.447×10^5 N/m^2 absolute pressure transducer and jet total pressure with a 3.447×10^5 N/m^2 pressure transducer. Survey static pressures were measured on a 3.447×10^4 N/m^2 absolute pressure transducer. All pressures except tunnel-wall static pressures were recorded on automatic balance potentiometers. The tunnel-wall static pressures, used to compute free-stream Mach number with the known tunnel total pressure, were read on mercury monometers and recorded periodically during each test run.

Survey Procedure

Data consisting of pitot pressure, static pressure, and volumetric hydrogen concentration were taken at downstream locations of 7, 30, 60, 120, and 200 injector nozzle exit diameters. At each station, data were taken at the test conditions indicated in the following table.

Test condition	x/d = 7	30	60	120	200
1	X	X	X	X	
2	X		X	X	
3	X	X	X	X	X
4	X	X	X	X	X

At each of the indicated conditions, one vertical and three horizontal surveys were made of the flow field. The vertical survey was made along the jet centerline stepwise from the plate surface outward until a zero hydrogen concentration was obtained. Horizontal surveys were made at points above the plate corresponding to maximum and half-maximum concentration and at a point midway between the plate surface and the point of maximum concentration.

For each horizontal survey, the positive edge (see coordinate system in fig. 1) of the mixing region was located. A stepwise survey was made across the flow field from this point until a hydrogen volume fraction of zero was obtained. At each point in the survey a gas sample and a pitot pressure measurement were taken. While the gas sample was being analyzed, the probe was moved to the next point and the sample line flushed prior to the introduction of a new sample. In regions of low pitot pressure, a diaphragm-type vacuum pump was used to withdraw the sample from the tunnel. The sample flow rate was throttled to maintain it constant.

Prior to and periodically during each set of surveys, hydrogen was drawn from the supply line and analyzed and the chromatograph readout attenuated to full-scale deflection. Repeatability was checked to a variation of less than 1/2 of 1 percent full scale.

Data Reduction and Accuracy

The raw pressure and concentration data at each survey point of each set of surveys - one vertical and three horizontal - were reduced to yield values of mass fraction, mixture molecular weight, Mach number, mixture total and static temperature, velocity, mixture and air mass flux, hydrogen mass flow parameter, and the nondimensional coordinates. The molecular weight of the hydrogen-air mixture was computed assuming molecular weights of the components of 2.016 and 29.0, respectively. Mixture total temperature was obtained from the mixture mass averaged total enthalpy computed from the measured total temperatures. The mixture was assumed to be a perfect gas and the values of Mach number, static temperature, and velocity computed using the equations for one-dimensional isentropic flow presented in reference 13. Local density of the mixture, used to compute the mass flux parameters, was calculated using the ideal gas equation of state with the universal gas constant equal to 1.986 cal/mole-$^{\circ}$K.

Before each set of surveys was made, the probe tip was positioned along the tunnel centerline on the plate surface. Vertical surveys were made at this probe location and it was the zero reference point for the horizontal surveys which were made by yawing the probe. During the course of the tests, it was determined that the centerline of the hydrogen-air flow field was not always coincident with the tunnel centerline. This is believed to be a result of the small scale of the injector, probe tip, and slight asymmetries of the tunnel flow. The maximum concentration was therefore sometimes obtained at a point to either side of the vertical survey location. When this occurred, the y/d location at which all of the horizontal concentration surveys peaked was taken as the true centerline ($y/d = 0$) and the vertical survey considered to have been made at a point slightly off-center. In most cases the distance between the tunnel and flow field centerlines, $(y/d)_{\alpha}$, was less than one injector diameter. Probe position accuracy of the actuator mechanism in the vertical surveys was ± 0.127 mm, the same as the probe tip height. This corresponds to an error in the vertical probe position of ± 0.125 injector diameters.

Since the horizontal surveys were made by yawing the probe, the x/d position of the probe tip is slightly greater at the edges than at the center of the mixing region. At the widest survey location, the change in the x position was less than two injector diameters.

VIII. RESULTS AND DISCUSSION

Flow Field Structure

The general structure of the flow field resulting from the normal sonic injection of hydrogen in a supersonic airstream is presented in figure 6. Flow conditions correspond to a q_r of 1.0 which gives a value of the jet exit static pressure of 1.4 atmospheres. The bow shock downstream of an x/d of 20 was determined from schlieren photographs and is essentially a Mach line. Its shape is not appreciably affected by a change in q_r. Details of the jet structure and bow shock in the vicinity of the injector are not clear because of the small-scale and thick boundary layer. Details of the boundary-layer separation and jet shock structure are presented in references 5, 6, and 8 for boundary layers on the order of one injector-diameter thick and larger values of q_r than those of the present investigation. The severity of the separation depends on the boundary-layer thickness relative to the injector diameter and the amount of underexpansion of the jet. Injection through a thick boundary layer, though having a greater penetration, would be turned downstream somewhat before encountering the high-velocity mainstream and would result in a weaker bow shock in the free stream. The injector back pressure would therefore be less for injection in thick boundary layers than in thin boundary layers. Reference 8 used a criterion for matched injection by defining an effective back pressure, p_b, as equal to two-thirds of the free-stream pitot pressure. For the conditions in figure 6, p_b is 1.27 atmospheres according to this criterion. Since a sonic injector cannot operate overexpanded, a matched pressure condition is the minimum pressure for operation. Investigation of the injector operation over a range of jet total pressures indicated that the jet measured mass flow rate was a linear function of the jet total pressure and, therefore, the jet maintained sonic operation, down to a value of $p_{t,j}$ corresponding to a q_r of approximately 0.45. This corresponds to a jet exit static pressure, and thus an effective back pressure of 0.63 atmosphere. For operation in the thick boundary layer of this investigation, with a Mach 4 free stream, the effective back pressure is approximately 40 percent of the free-stream pitot pressure. It is believed that this result differs substantially from that of reference 8 because of the relatively thicker boundary layer of the present investigation.

The data shown in figure 6 are profiles of hydrogen mass fraction taken in vertical surveys behind the jet centerline. Trajectories are shown for the line of maximum concentration, half-maximum concentration, and the point at which the volume fraction is half of 1 percent. As can be seen, the hydrogen jet is rapidly turned downstream by the free stream and mixes rapidly in the near field, the maximum concentration decreasing to about 12 percent mass fraction in seven injector diameters. From an x/d of 7 to x/d of 60, the mixing is slower with the maximum concentration decreasing by about 60 percent. The major part of the jet penetration into the airstream occurs within seven injector diameters. For the thick boundary layer, $\delta/d = 2.70$, and low values of q_r, the mixing region remains almost entirely embedded in the boundary layer.

Effect of dynamic pressure ratio on jet initial penetration.- The penetration of a gaseous jet into a supersonic free stream has been greatly discussed in the literature. Zukowski and Spaid (ref. 5) and Spaid, et al. (ref. 6) define penetration as the point at which maximum concentration occurs, while Vranos and Nolan (ref. 7) and Orth, et al. (ref. 8) consider penetration as the height above the plate at which the volume fraction is 0.005. As used herein, the term "penetration" will refer to the vertical edge of the mixing region and be denoted as $(z/d)_o$; the height at which the concentration is maximum is referred to as "penetration-to-α_{max}" and will be denoted $(z/d)_\alpha$.

Equations describing the penetration and α_{max} trajectories have been developed by correlating data (ref. 7) and are given here for normal, sonic, injection of hydrogen in a Mach 4.03 free stream.

$$(z/d)_o = 3.75\ q_r^{0.5}(x/d)^{0.0866} \tag{1}$$

$$(z/d)_\alpha = 3.45\ q_r^{0.533}(x/d)^{-0.259} \tag{2}$$

These equations were derived for data in the far field and are applicable for x/d greater than 7. Equations (1) and (2) are presented in figures 7 and 8 as solid lines with data from the present investigation. In figure 7 the effect of q_r on the initial penetration, at an x/d of 7, is illustrated. Equation (2) shows a reasonable agreement with the data, although it does predict slightly less penetration-to-α_{max} at the higher values of q_r. A straight line through the data points would have a slope of 0.6 compared to 0.533 for equation (2).

The penetration predicted by equation (1) is about 20 percent low at an x/d of 7 and has a slope of 0.5. A straight line through the penetration data points would have a slope of 0.3.

Figure 8 shows the α_{max} and penetration trajectories for a value of q_r of 1.0. Equation (1) predicts an outer boundary of the mixing region that increases from about 20 percent low at x/d of 7 to about 45 percent low at an x/d of 200. The α_{max} trajectory predicted by equation (2) approaches the plate at large values of x/d. Data show an initial decrease in the α_{max} trajectory to an x/d of 30 but an increase at stations farther downstream. Equations (1) and (2) were obtained for helium injected from a 0.478-centimeter exit diameter nozzle mounted normal to the wall of an 8.89-centimeter-diameter duct. The curvature of the wall and the possibility of interference from the opposite side of the duct could account for the discrepancies between the present data and the equations. Another correlation for the penetration of a normal jet and reported in reference 9 is

$$(z/d)_o = 1.446\ q_r^{0.392}(M_\infty/M_j)^{0.613}(x/d)^{0.0396+0.379\ M_j/M_\infty} \qquad (3)$$

For sonic injection in a Mach 4.03 free stream, the equation reduces to

$$(z/d)_o = 3.40\ q_r^{0.392}(x/d)^{0.134} \qquad (4)$$

Equation (3) was derived from data taken at free-stream Mach numbers of 1.6 and 3.0 over an x/d range of 14 to 167. The injected gas was simulated methane. The effect of boundary-layer thickness was not investigated. Equation (4) is presented in figures 7 and 8 as dashed lines and gives a better prediction of the penetration than equation (1). An equation derived from a correlation of the present data at values of x/d less than 120 - shown as a dashed line in figure 9(c) - is

$$(z/d)_o = 3.87\ q_r^{0.300}(x/d)^{0.143} \tag{5}$$

The slight differences in the constants of equations (4) and (5) could be due to the different injected gases and different boundary layers.

The broken lines in figures 7 and 8 are the results from a method presented in reference 8 for calculating the jet centerline trajectory (α_{max} trajectory) in the near field. This method considers the emerging jet as being composed of cylindrical elements of length d(h/d) with the aerodynamic drag on each element computed from empirical equations. The equation from reference 8 is

$$6.91\ q_r \int_{\theta}^{\theta_i} \frac{d\theta}{C_D(\theta)\ \sin^2(\theta)} = \left(0.22\ \frac{h}{d} + 2.25\right)^4 - 2.25^4 \tag{6}$$

where

$$C_D(\theta) = 1.2 + (M_\infty \sin\theta)^{7/2}, \qquad 0 \leq M_\infty \sin\theta \leq 1 \tag{7}$$

$$C_D(\theta) = 1.06 + 1.14(M_\infty \sin\theta)^{-3}, \qquad M_\infty \sin\theta \geq 1 \tag{8}$$

The integral is evaluated by selecting a value of θ and integrating to the initial value, θ_i. For normal injection, θ_i is 90°.

Equation (6) underpredicts the effect of q_r on the initial penetration at an x/d of 7, but again, the effect of boundary layer is not accounted for. Calculations were made using the mass averaged boundary-layer conditions rather than free stream in equation (6) with no significant change in the trajectory or the effect of q_r.

Effect of dynamic pressure ratio on the penetration trajectories.- Figure 9 presents the trajectories of maximum concentration, half-maximum concentration, and the penetration height, correlated with the jet-to-free-stream dynamic pressure ratio. For all values of q_r, except a value of 0.5, the penetration-to - α_{max} decreased with increasing x/d to an x/d of about 30, beyond which penetration-to - α_{max} increased. The minimum value of $(z/d)_\alpha$ occurred farther downstream the higher the value of q_r. In order to bring these minimum points together a factor $q_r^{-1.6}$ was applied to the x/d coordinate producing the family of curves presented in figure 9(a). The fact that the maximum concentration trajectory turned beyond parallel with the plate surface, as evidenced by the initial decrease in $(z/d)_\alpha$, is thought to be caused by the thick boundary layer. Figure 9(b) presents the trajectories of the point at which the mass concentration is one-half the maximum at each x/d station. At all downstream stations the $(z/d)_5$ coordinate was taken in that part of the flow field between the point of maximum concentration and the edge of the mixing region. The effect of q_r on the coordinates of these points is such that a factor of $q_r^{-0.8}$ applied to the x/d coordinate produces a family of curves similar to those for the $(z/d)_\alpha$ trajectories. The family of curves for the $(z/d)_\alpha$ and $(z/d)_5$ trajectories both show two distinct characteristics. For α_{max} trajectory family, the data points essentially lie on a straight line of negative slope at values of the x coordinate less than 30. Downstream of this minimum point the α_{max} trajectories diverge with the slope increasing for increasing values of q_r. The half-maximum trajectories exhibit similar properties with the dividing point, for a q_r of 1.0, occurring near a value of x/d of 15. At all x/d stations, an increase in q_r produced a proportional increase in $(z/d)_o$ such that the individual trajectories were brought together by multiplying the $(z/d)_o$ coordinate by $q_r^{-0.3}$ as shown in figure 9(c). The solid line is a fairing through the data points; the dashed line is a straight-line approximation to the penetration trajectory at values of x/d less than 120, and is represented by equation (5).

Decay of maximum concentration.- The decay of the maximum concentration as a function of x/d_j and q_r is presented in figure 10. The effect of q_r was found to be such that a factor of $q_r^{-1/2}$ multiplied by the x/d_j coordinate provided a reasonable correlation. Downstream of an x/d of 30 the concentration decay may be represented by a straight line with a slope of -0.8; that is, the decay of α_{max} is inversely proportional to $(x/d_j)^{0.8}$. Extrapolating this straight line - shown as a dashed line in figure 10 - to a value of α_{max} of 1.0 yields a length equivalent to the potential core in coaxial flow. For values of q_r from 0.5 to 1.5, the equivalent potential core length ranges from 1.2 to 2.2 jet diameters. Compared to coaxial flow the mixing for normal injection is much faster in the near field, yet slower in the far field. As reported in reference 2, the concentration decay in the far field for coaxial mixing is inversely proportional to x^2.

Presentation of Data

Profiles of concentration, velocity, and total pressure were nondimensionalized for the vertical survey and the horizontal survey through the point of maximum concentration at values of q_r of 0.5, 1.0, and 1.5 and all x/d stations. These profiles are presented in figures 11 through 13 for the vertical surveys and figures 14 through 16 for the horizontal surveys.

Vertical survey profiles.- For each vertical survey the largest value of mass concentration, α_{ref}, and the corresponding value of z/d were obtained by fairing a curve through the data points. The value of α is not necessarily the maximum concentration due to the uncertainty of aligning the sample probe with the jet centerline (see the Data Reduction and Accuracy Section).

The concentration profiles normalized by α_{ref} and with the origin of the coordinate system shifted to $(z/d) = (z/d)_{ref}$ are presented in figure 11 for each value of x/d. At values of z/d greater than the value of z/d at α_{ref}, the vertical coordinate was nondimensionalized by the distance from the point of α_{ref} to the edge of the mixing region, $(z/d)_o - (z/d)_{ref}$. At values of z/d less than $(z/d)_{ref}$, the vertical coordinate was nondimensionalized by $(z/d)_{ref}$.

For z/d greater than $(z/d)_{ref}$, a change in the value of q_r has negligible effect on the shape of the profile. However, the profile shape does change with x/d. To compare the shape of the profiles at values of z/d greater than $(z/d)_{ref}$ as the mixing progresses downstream, a Gaussian-type exponential curve of the form

$$\frac{\alpha}{\alpha_{ref}} = \exp\left\{-5\left[\frac{z/d - (z/d)_{ref}}{(z/d)_o - (z/d)_{ref}}\right]^{b_1}\right\} \tag{9}$$

is shown for each x/d. The value of b_1, the vertical profile shape index, required to give a reasonable fit of equation (9) with the data is given in the tables in figure 11. At x/d stations downstream of 30, the value of b_1 is constant at a value of 2.70, indicating that the flow field has become fully developed. This may be associated with the fact that the maximum concentration trajectory in figure 9 has a minimum near a value of $(x/d)q_r^{-1.6}$ of 30 and that the maximum concentration decay in figure 10 has a constant slope downstream of an x/d of 30.

The portion of the profiles at values of z/d less than $(z/d)_{ref}$ show no predictable effect of q_r. However, at values of x/d less than 60 the slope of the lower half of the profiles increases, in general, with an increase in q_r. That is, in the vicinity of the plate surface the mixing region is generally more uniform at the lower values of q_r. The slope of the profiles near the plate surface decreases with increasing x/d. At an x/d of 60 and above, curves faired through the data points would intersect with the plate surface at values of α/α_{ref} between 0.6 and 0.7 for all values of q_r.

The nondimensional velocity profiles are presented in figure 12 for all x/d stations at each value of q_r. Also shown for comparison is the undisturbed boundary-layer profile taken at the injector exit station (see fig. 2). For each data profile, the value V_o is the velocity at the edge of the mixing region at a height $(z/d)_o$ above the plate. For the boundary-layer profiles $V_o = V_\infty$ and $(z/d)_o = \delta$. At x/d stations of 7 and 30, the effect of increasing q_r can be seen as an increase in the peak velocity located within the profiles. This is due to the fact that for constant initial conditions the mass flow rate of injected gas increases directly with q_r so that there is more high-velocity hydrogen near the injector at the higher values of q_r. The initial jet-to-free-stream velocity ratio is approximately 2. At values of x/d downstream of 30, the shape of the velocity profiles approach that of the boundary layer, the higher values of q_r requiring a greater length.

The quantity z_1 in the tables of figures 12 and 13 is the height of the undisturbed streamtube upstream of the injector that contains the same mass flow of air as the mixing region downstream. It was computed by assuming that the undisturbed streamtube has the same cross-sectional shape as the mixing region and will be discussed later in more detail. For the boundary-layer survey, $z_1 = \delta$. Each profile then represents a segment of boundary-layer-type flow with a thickness of z_1 when referenced to the undisturbed flow.

Nondimensional total pressure profiles corresponding to the same conditions as the velocity profiles are presented in figure 13. The boundary-layer total pressure profile from figure 2 is also included for comparison. As with the velocity profiles, the total pressure profiles at stations far downstream approach the same shape as the boundary-layer profiles. However, near the edge of the mixing region, at large values of x/d, the slope of the total pressure profiles is larger than the boundary-layer profile. The total pressure at the edge of the mixing region generally increases with increasing x/d. This is due to an addition to the mixing region of free-stream air that has passed through a weaker portion of the bow wave. All of the profiles exhibit the same degree of total pressure loss due to the loss in momentum required to turn and accelerate the injected hydrogen. This region of low total pressure extends over approximately 60 percent of the vertical height of the flow fields and is most severe at the upstream stations.

Horizontal survey profiles.- Nondimensional concentration profiles for the horizontal survey through the point of maximum concentration are presented in figure 14. Here the concentration is normalized by the maximum value which occurred a distance $(y/d)_\alpha$ from the tunnel centerline, or the point at which the vertical survey was taken. The lateral coordinate is nondimensionalized by the average distance from the centerline to each of the lateral edges of the mixing region, $(\overline{y/d})_o$. The values of $(\overline{y/d})_o$ have a somewhat random variation varying from roughly 5 to 8 from an x/d of 7 to 200 with a ±20 percent deviation at a given station. As with the vertical surveys, the dynamic pressure ratio has little or no effect on the profile shape at each x/d. To compare the effect of x/d on the profile shape, a Gaussian-type exponential curve is presented. The equation is of the form

$$\frac{\alpha}{\alpha_{max}} = \exp\left\{-5\left[\frac{y/d - (y/d)_\alpha}{(\bar{y}/d)_o}\right]^{b_2}\right\} \tag{10}$$

where b_2 is the horizontal profile shape index. The values of b_2 required to give a fit of equation (10) with the data are given in the tables in figure 14. At values of x/d of 7, 30, and 60, b_2 is constant at a value of 1.5 and increases to a value of 2.0 at an x/d of 200. Equation (10) fits the data reasonably well, especially at an x/d of 120 and 200.

The velocity profiles for the horizontal surveys are presented in figure 15. The velocity, V_o, used to nondimensionalize the data points has the same value as that used for the vertical surveys in figure 12. For absolute values of $\frac{\left[y/d - (y/d)_\alpha\right]}{(\bar{y}/d)_o}$ greater than 0.5, the profiles are fairly uniform with the level of the velocity ratio, more a function of the value of z/d at which the survey was made than it is x/d. Generally, in the outer part of the flow field the velocity increases with increasing z/d. Near the center of the mixing region - absolute values of the y coordinate less than 0.5 - the velocity level decreases with increasing x/d. Thus, as the mixing progresses downstream, the velocity profiles, instead of having a maximum near the center of the flow field, have a minimum. This is a result of the flow field becoming established at large values of x/d as indicated in figure 12 by the vertical velocity surveys approaching the shape of the undisturbed boundary layer.

Profiles of total pressure for the horizontal surveys are presented in figure 16. As with the velocity profiles, the total pressure profiles exhibit different trends near the edge of the flow field than near the center. Near the edge of the mixing region, the level of pressure increases with increasing z/d, while in the vicinity of the centerline, the pressure level is a function of x/d and, in general, increases monotonically with x/d. As the mixing progresses downstream, the pressure profiles become steeper as a result of higher momentum air being added to the mixing regions at the edges. The pressure level at the centerline never recovers from the injection disturbance and is less than 8 percent of free-stream total pressure even at 200 injector diameters downstream.

Flow Field Contours

Contours of mass fraction, hydrogen mass flow rate parameter, and air mass flow parameter were obtained by cross-plotting the vertical and horizontal profiles at constant values of the particular parameter. Contours of α and β are presented in figures 18 and 19, respectively; contours of ξ are not presented, but the results of the integration of the contours performed as a continuity check and an indication of the overall accuracy of the data are given in figure 17. The contours of fuel mass flow were plotted in the nondimensional form

ξ/ξ_{max} where ξ_{max} is the maximum value for each set of surveys and generally occurred near the point of α_{max}. In terms of ξ, the integrated mass flow rate of hydrogen is

$$\dot{m}_{int} = (\rho V)_j \xi_{max} \int_0^{A_o} (\xi/\xi_{max}) dA \tag{11}$$

Dividing equation (11) by A_o and the measured hydrogen mass flow rate, $\dot{m}_j = \frac{\pi(\rho V)_j d_j^2}{4}$ gives

$$\frac{\dot{m}_{int}}{\dot{m}_j} = \frac{4\xi_{max} A_o}{\pi d_j^2} \int_0^{1.0} \left(\frac{\xi}{\xi_{max}}\right) d\left(\frac{A}{A_o}\right) \tag{12}$$

as the ratio of integrated-to-measured hydrogen mass flow. Results of evaluating equation (12) at the various downstream stations are given in figure 17. The solid symbols in figure 17 represent the average deviation of equation (12) from unity. As can be seen, the accuracy of the data is better at the far downstream stations. At all values of x/d, the deviation of equation (12) from unity increases with increasing values of q_r. This is probably due to the larger gradients in the concentration and velocity - which are associated with the local turbulence level - produced by the stronger jet at the higher values of q_r. The characteristics of a binary gas flow field that affect the accuracy of concentration measurement are discussed in reference 3. Accuracy of concentration measurements in a flow field composed of gases with a large difference in molecular weights is also affected by the sampling probe-tip geometry. An investigation reported in reference 14 for subsonic flow of coaxial jets indicated that a probe tip with a rapid internal expansion provided better results than one with a long length of constant internal area when compared to measured mass flow rates. Reference 3 indicated that the probe and sampling lines should be free of any obstruction so that the probe tip will operate at nearly full capture. For flow fields of this nature, differences between integrated and measured mass flow rates of 20 percent are considered typical.

The contours represent cross sections of the flow field in the y-z plane and are bounded by the contour for a concentration of zero which defines the outer edge of the mixing region. Above a value of z/d of about 3 the zero concentration contour may be approximated by a semicircle with the center at the point of maximum concentration. Below a z/d of approximately 3 the zero concentration contour rapidly spreads laterally in the boundary layer.

For each value of q_r the overall width of the $\alpha = 0$ contours is essentially constant at x/d stations downstream of 30. The height of the contour, which is approximately the penetration, almost doubles from an x/d of 7 to an x/d of 200. The contours for a particular value of α other than $\alpha = 0$ decrease in area with increasing x/d and decreasing value of q_r as shown in figure 18.

The air mass flow rate contours in the nondimensional form β/β_{max} and contained within the $\alpha = 0$ contour are presented in figure 19. The intersections of the β/β_{max} contour and the $\alpha = 0$ contour were determined by plotting the value of β at the point in the horizontal surveys where $\alpha = 0$ as a function of z/d and interpolating to find the coordinate corresponding to a particular value of β/β_{max}. The mass flow rate of air contained within the mixing region was obtained by evaluating the integral

$$\dot{m}_1 = \beta_{max} A_o \int_0^{1.0} (\beta/\beta_{max}) d(A/A_o) \tag{13}$$

where A is the cross-section area bounded by each β/β_{max} contour and A_o is the cross-section area within the $\alpha = 0$ contour. Results of the integrations were used to determine the average fuel-air ratio and the size of the undisturbed streamtube upstream of the injector that contains the same air mass flow rate as the mixing region downstream.

The undisturbed streamtube area, A_1, was calculated for each x/d and q_r by assuming that it was of the same shape as A_o. That is, the ratio of the height, z_1, to the average width, $y_1 = A_1/z_1$, of the streamtube was assumed constant. This gives the following equation for A_1:

$$A_1 = A_o (z_1/z_o)^2 \tag{14}$$

The height of the undisturbed streamtube was calculated from the continuity equation and the definition of boundary-layer displacement thickness

$$\dot{m}_1 = \int (\rho V) dA = (\rho V)_\infty (z_1 - \delta^*) y_1 \tag{15}$$

but

$$y_1 \doteq A_1/z_1 = A_o z_1/z_o^2 \tag{16}$$

Substituting equation (16) into (15) and solving the resulting quadratic for z_1 gives

$$z_1 = \frac{\delta^*}{2} + \left[\left(\frac{\delta^*}{2}\right)^2 + \frac{\dot{m}_1 z_o^2}{(\rho V)_\infty A_o}\right]^{1/2} \tag{17}$$

Values of z_1 obtained from equation (17) for the integrated air mass flows of equation (13) are given in the tables of figures 12 and 13. In application to the design of supersonic combustors, the size and shape of the undisturbed streamtube provides information as to the spacing of injectors and the injector size to obtain penetration to the combustor centerline. If a stoichiometric value of $\bar{f}$ is desired the combustor entrance must have a half-height equal to the value of z_1 that corresponds to the x/d station at which a stoichiometric average fuel-air ratio was obtained. Confining the flow field by the addition of an opposite wall would be expected to change the mixing rate and penetration from that presented herein but would yield the same average fuel-air ratio. The injector spacing is the average width of the undisturbed streamtube, y_1. An estimation of these parameters is discussed in the next section.

Estimation of Cold Flow Mixing Parameters

The mixing length relative to the combustor entrance height and the injector spacing required to give a stoichiometric average fuel-air ratio ($\bar{f} = 0.0293$ for hydrogen in air) has been estimated by superimposing the flow field cross section of a single injector. A schematic for a two-dimensional configuration with staggered injection from both walls is presented in figure 20. It is assumed that a particular concentration contour from the single jet flow field coincides with the same contour of the adjacent and opposite injectors. For the purposes of this discussion, it is assumed that the superimposed flow field is coincident along the contours of half-maximum concentration, shown as dashed lines in figure 20. It follows that the air mass flow that mixes with the hydrogen from one injector is contained within the half - α_{max} contour, since the area bounded by the adjacent contours covers the entire cross section of the combustor. Denoting the area contained by the half - α_{max} contour as A_5, equation (13), for the air mass flow, becomes

$$\dot{m}_1 = \beta_{max} A_5 \int_0^{1.0} (\beta/\beta_{max}) d(A/A_5) \qquad (18)$$

The height and width of the confined air streamtube are given by equations (17) and (16) by replacing A_o and z_o with A_5 and z_5, respectively.

Values of average fuel-air ratio obtained from the total injected hydrogen mass flow and the integrated air mass flow for the unconfined jet (eq. (13)) and the α/α_{max} of 0.5 contour (eq. (18)) are presented in figure 21 as a function of x/d_j and q_r. The effect of q_r on the decay of $\bar{f}$ for both conditions was found to be such that a factor of $q_r^{-1/2}$ provided a reasonable correlation. For the unconfined jet the value of $\bar{f}_o$ is below stoichiometric for all x/d stations considered. Downstream of 30 injector diameters, the decay of $\bar{f}_o$ is inversely proportional to approximately $(x/d_j)^{0.6}$. For the case of simulated opposite wall injection the average fuel-air ratio, $\bar{f}_5$, is considerably higher than $\bar{f}_o$ and becomes stoichiometric at an x/d_j of 200 for a q_r of 1.0. It is apparent that the lowest value of q_r will provide a stoichiometric average fuel-air ratio in the shortest distance. Also, using a coincident concentration contour with a value less than half maximum would yield a stoichiometric value of $\bar{f}$ at a shorter x/d since the resulting curve for the decay of $\bar{f}$ would lie somewhere between the curves for $\bar{f}_o$ and $\bar{f}_5$. However, the uniformity of the flow field would need to be investigated to select the optimum value.

To determine the combustor size, the average fuel-air ratio of the simulated combustor flow field is plotted in figure 22 as a function of x/z_1. The value of z_1 represents the combustor entrance half-height. From figure 22, $\bar{f}_5$ is stoichiometric at a value of x/z_1 of approximately 40. The hydraulic diameter of a two-dimensional duct is twice the duct height, or $4z_1$. The mixing length required for a stoichiometric average fuel-air ratio is approximately 10 hydraulic diameters, which agrees with values used for engine design. For a q_r

of 0.5, the value of z_1 for a stoichiometric value of $\bar{f}_5$ is approximately 3.3 injector diameters - corresponding to an x/d_j of 140 from figure 21. The value of y_1, which is the required injector spacing corresponding to these conditions, is approximately 3.0 injector diameters.

IX. CONCLUDING REMARKS

Comparisons of the present data to data correlations from other sources indicated a significant effect of the thick boundary layer on the initial penetration of the jet, the downstream trajectories, the jet effective back pressure, and probably the mixing rate. All the data correlations underpredicted the effect of jet-to-free-stream dynamic pressure ratio on the initial penetration and the penetration trajectory. Equation (3) from reference 9 provided the best agreement to the present data which correlated as a function of $q_r^{0.3}$. The trajectory for the penetration-to-α_{max} was initially turned beyond parallel to the plate surface and then increased monotonically with the slope of the trajectories increasing with dynamic pressure ratio. Minimum values of $(z/d)_\alpha$ occurred at values of x/d ranging from 9 to 45 for values of q_r between 0.5 and 1.5, respectively. As a consequence of the overturning of the maximum and half-maximum concentration trajectories, simple empirical data correlations are not possible.

Investigation of the jet operation over a range of pressures indicated that the jet effective back pressure - the minimum jet exit static pressure for a sonic injector - for operation in the thick boundary layer of this investigation is approximately 40 percent of free-stream pitot pressure.

From the level of the measured maximum concentration near the injection station, it can be concluded that the turning and initial mixing of the hydrogen jet is very rapid. Downstream of an x/d of 30, the decay of the maximum concentration is inversely proportional to $(x/d_j)^{0.8}$, which is a slower mixing rate than coaxial mixing in the far field. Mixing in the near field is much faster for normal injection. The equivalent potential core lengths for normal injection were estimated to range from 1.2 to 2.2 jet diameters for values of q_r between 0.5 and 1.5, respectively.

Examination of concentration profiles on the vertical centerline suggest that the profile shape above the point of maximum concentration is not dependent on the dynamic pressure ratio and may be represented by a Gaussian-type function. The profiles show similarity at values of x/d equal to or greater than 60 and are nonsimilar at values of x/d of 7 and 30. Horizontal concentration profiles through the point of maximum concentration are also represented by a Gaussian-type function and exhibit similarity at values of x/d less than 60.

The loss in momentum and total pressure of the airstream, caused by turning and accelerating the hydrogen jet, resulted in an extensive region of very low total pressure. The region extended over 60 percent of the height near the center of the flow field and 40 percent of the width with a total pressure less than 10 percent of the free stream even at 200 injector diameters downstream.

Investigations of the mixing patterns at each station to obtain overall data discrepancies as judged by the measured fuel flow indicated a general trend of large discrepancies at upstream stations where values of the maximum concentration were high, and discrepancies approaching zero at downstream stations where α_{max} was near stoichiometric.

X. BIBLIOGRAPHY

1. Anon.: Statement of Work, Hypersonic Ramjet Experiment Project for Phase I. Langley Research Center, L-4947, 1965.

2. Henry, J. R.; and McLellan, C. H.: The Air-Breathing Launch Vehicle for Earth Orbit Shuttle - New Technology and Development Approach. AIAA Advanced Space Transportation Meeting, Cocoa Beach, Fla., Feb. 4-6, 1970.

3. Eggers, J. M.; and Torrence, M. G.: An Experimental Investigation of the Mixing of Compressible Jets in a Coaxial Configuration. NASA TN D-5315, 1969.

4. Torrence, M. G.: Concentration Measurements of an Injected Gas in a Supersonic Stream. NASA TN D-3860, 1967.

5. Zukowski, E. E.; and Spaid, F. W.: Secondary Injection of Gases Into a Supersonic Flow. Karman Lab. of Fluid Mech. and Jet Prop., California Institute of Technology, 1963.

6. Spaid, F. W.; Zukowski, E. E.; and Rosen, R.: A Study of Secondary Injection of Gases Into a Supersonic Flow. Jet Prop. Lab. Tech. Report No. 32-834, 1966.

7. Vranos, A.; and Nolan, J. J.: Supersonic Mixing of Helium and Air. Bumblebee Report TG 63-53, Appl. Phys. Lab., Johns Hopkins Univ., 1964, pp. 131-161.

8. Orth, R. C.; Schetz, J. A.; and Billig, F. S.: The Interaction and Penetration of Gaseous Jets in Supersonic Flow. NASA CR 1386, 1969.

9. Faucher, J. A., Jr.; Goldstein, S.; and Tabach, E.: Supersonic Combustion of Fuels Other Than Hydrogen for Scramjet Application. Pratt and Whitney Aircraft Div. U.A.C., Tech. Rept. AFAPL-TR-67-12, 1967, pp. 57-74.

10. Henry, J. R., et al.: Boundary Layer and Starting Problems on a Short Axisymmetric Scramjet Inlet. Compressible Turbulent Boundary Layers, Symposium at Langley Research Center, 1968.

11. Jeffrey, P. G.; and Kipping, P. J.: Gas Analysis by Gas Chromatography. The Macmillian Co., c. 1964.

12. Harris, W. E.; and Habgood, H. W.: Programed Temperature Gas Chromatography. John Wiley and Sons, Inc., c. 1966.

13. Anon.: Equations, Tables, and Charts for Compressible Flow. NASA TR 1135, 1953.

14. Alpinieri, L. J.: An Experimental Investigation of the Turbulent Mixing of Non-Homogeneous Coaxial Jets. PIBAL Report No. 789 (Contract No. AF 49(638)-217), Polytech. Inst., Brooklyn, August 1963.

XI. VITA

The author was born in [redacted], [redacted], on [redacted], [redacted], and received his primary and secondary education in public schools in Augusta. In 1963, after graduating from Augusta College with the degree of Associate of Science, he entered the Georgia Institute of Technology from which he was granted the degree of Bachelor of Aerospace Engineering, with honor, in June 1965. Since then he has been employed in a research capacity at Langley Research Center of the National Aeronautics and Space Administration.

R. Clayton Rogers

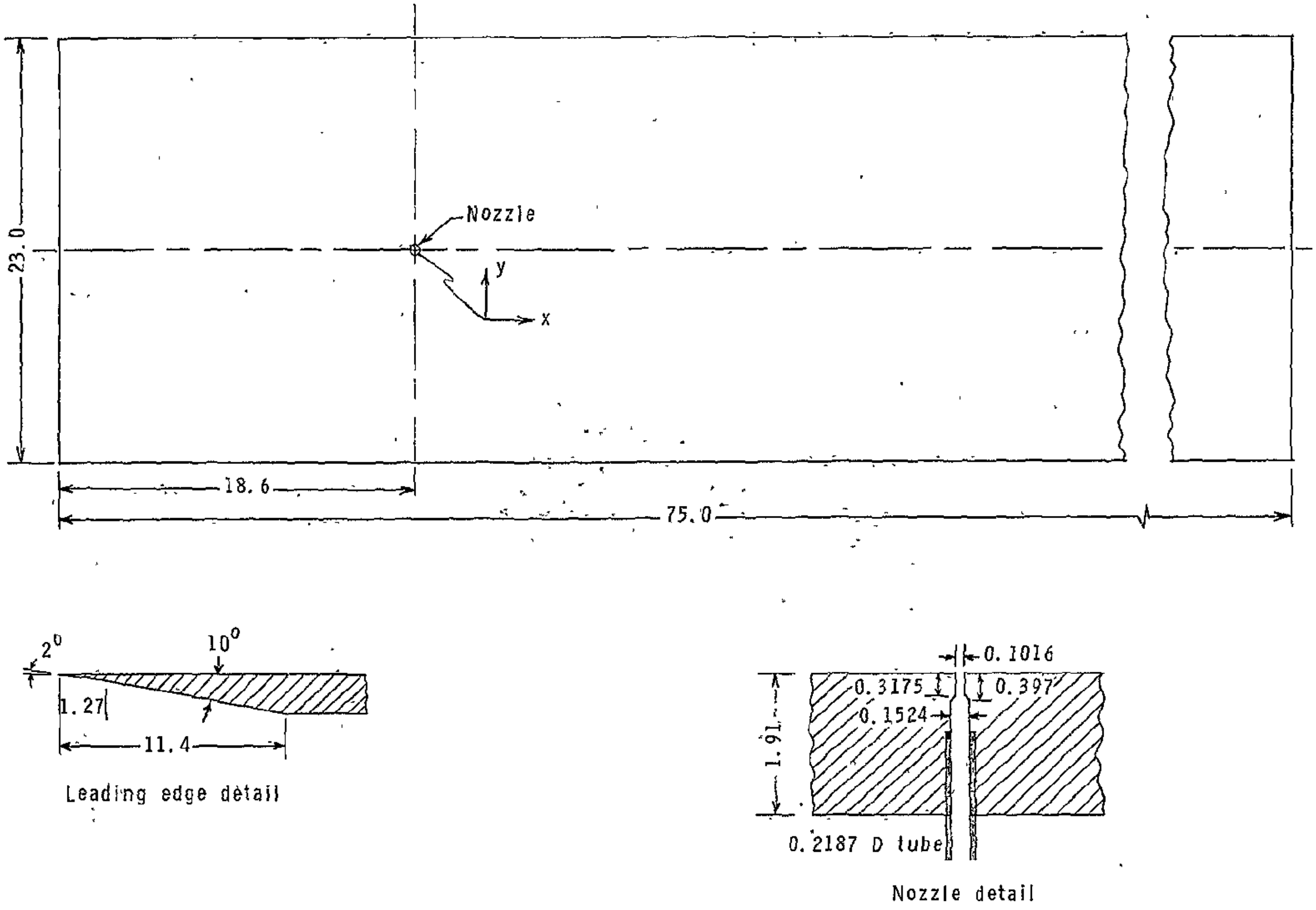

Figure 1.- Sketch of model. All dimensions in centimeters.

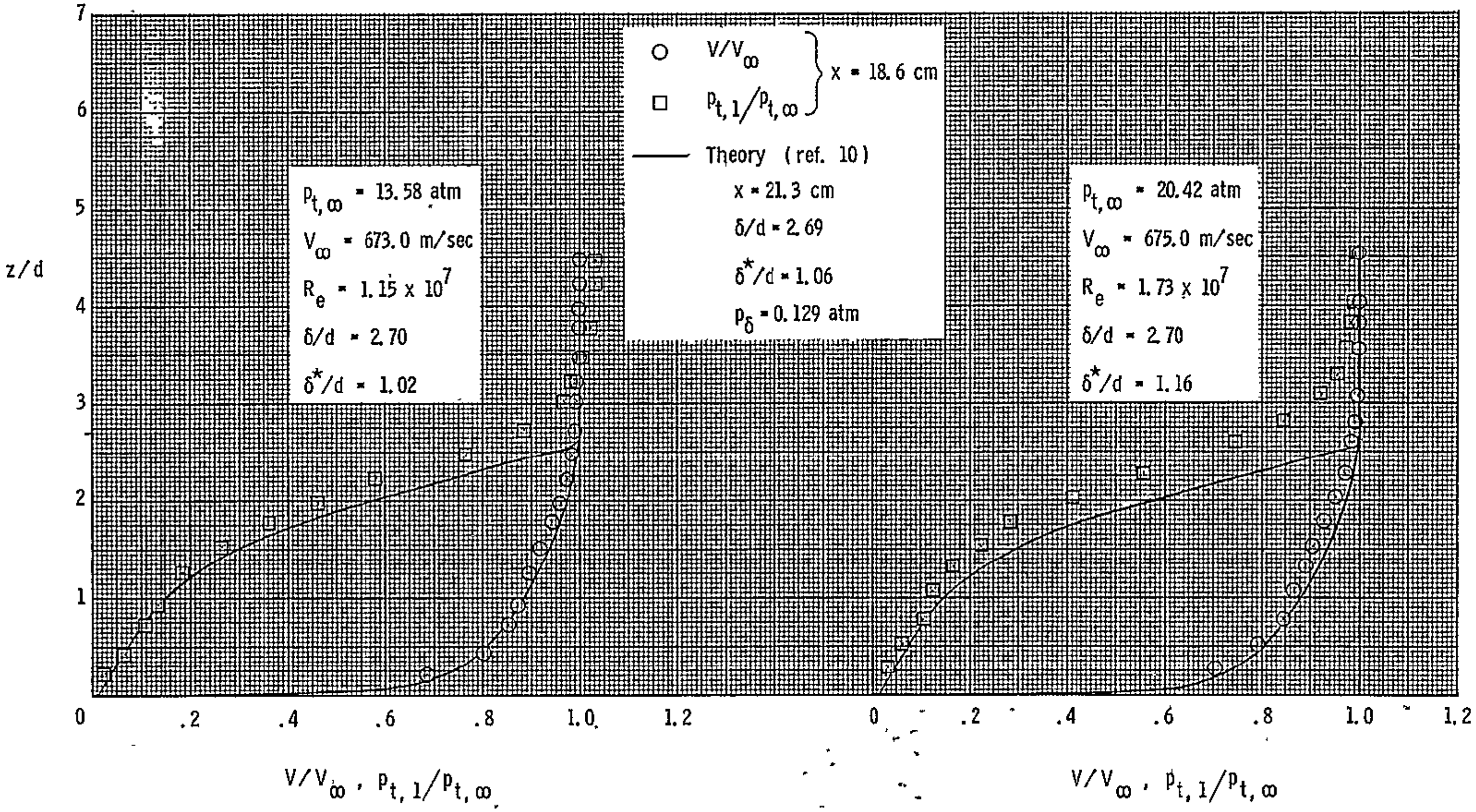

Figure 2.- Boundary layer surveys on flat plate model at injector exit station; no injection.

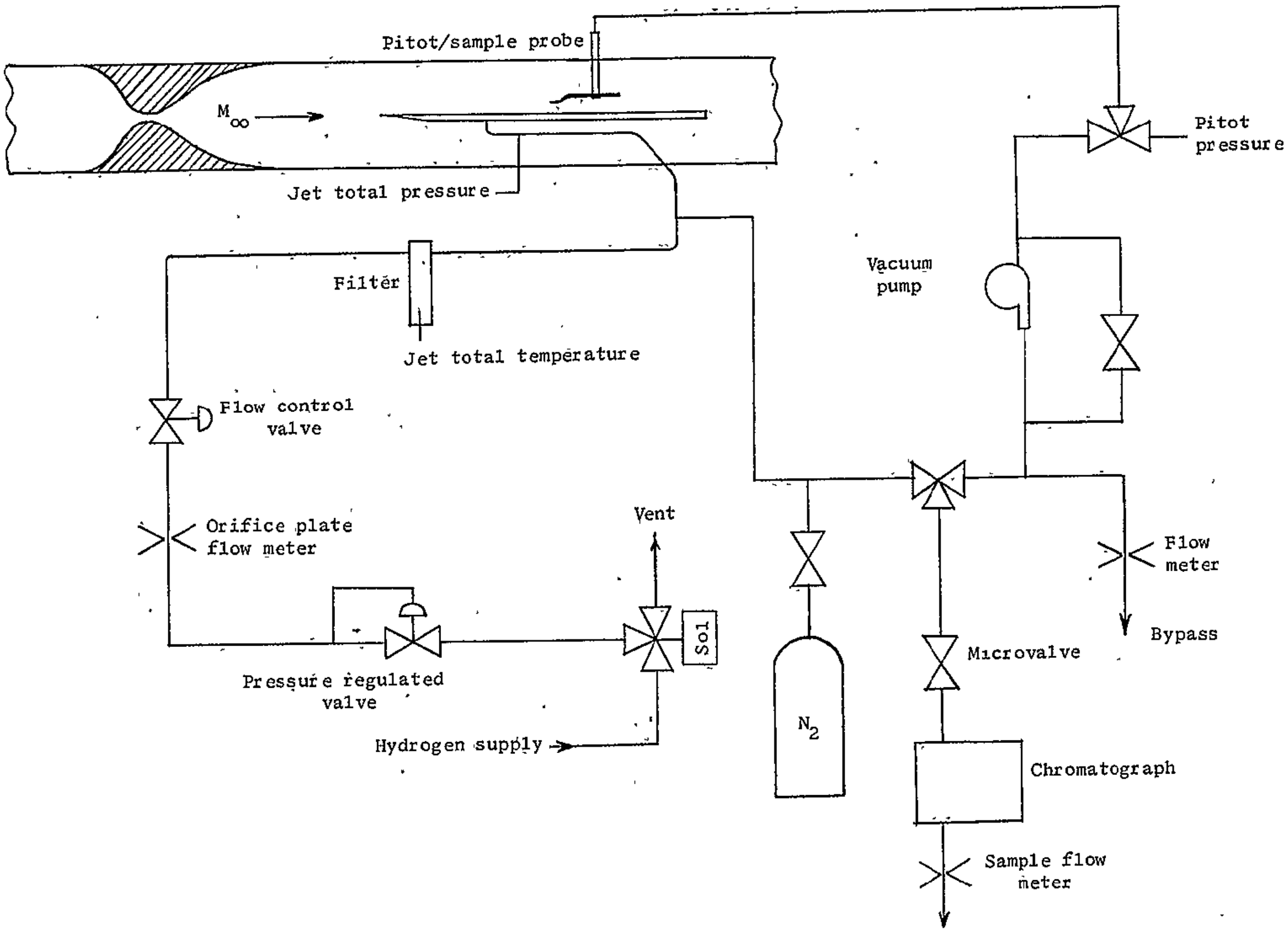

Figure 3.- Tunnel and secondary flow schematic.

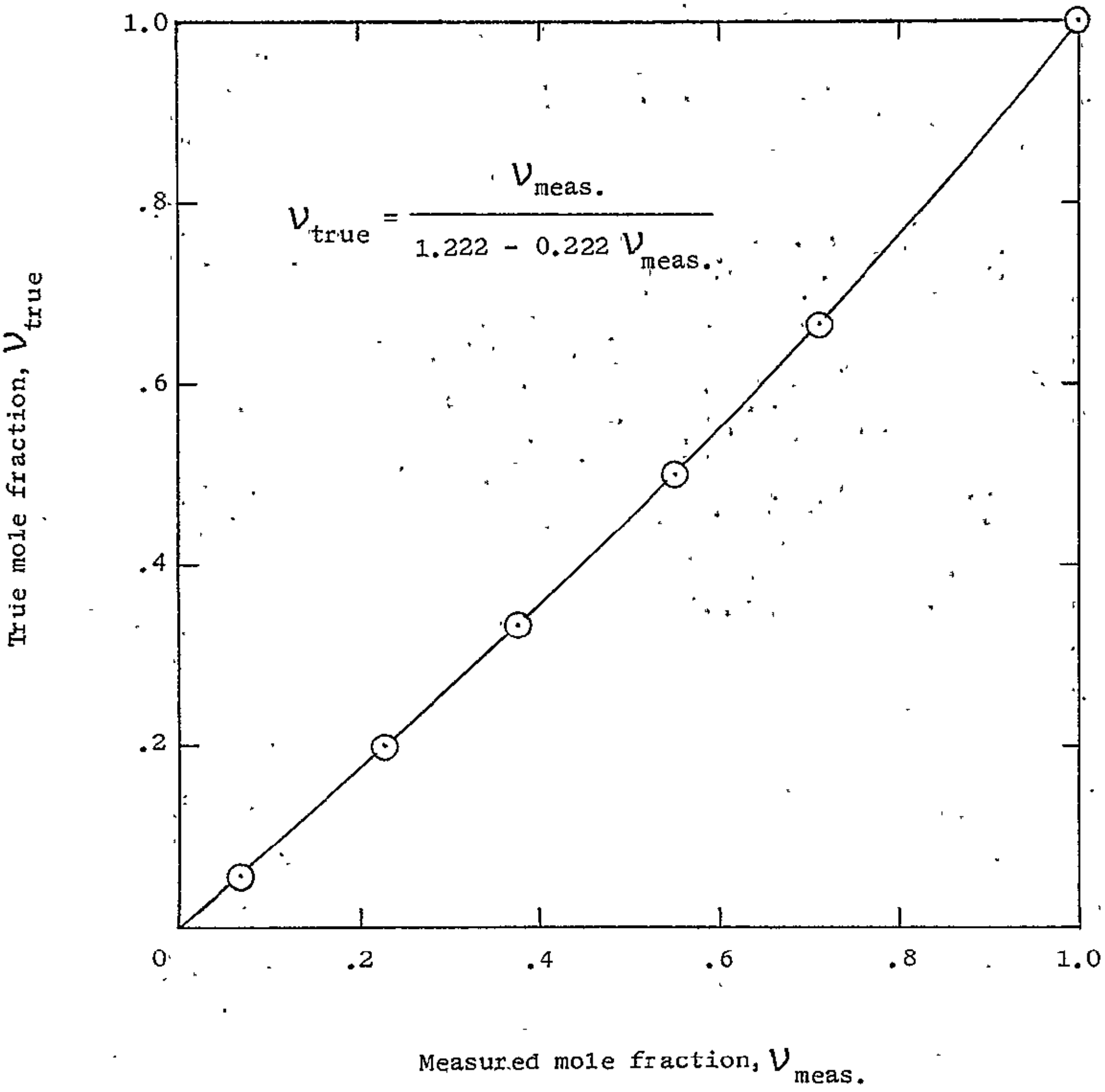

Figure 4.- Gas chromatograph calibration for hydrogen.

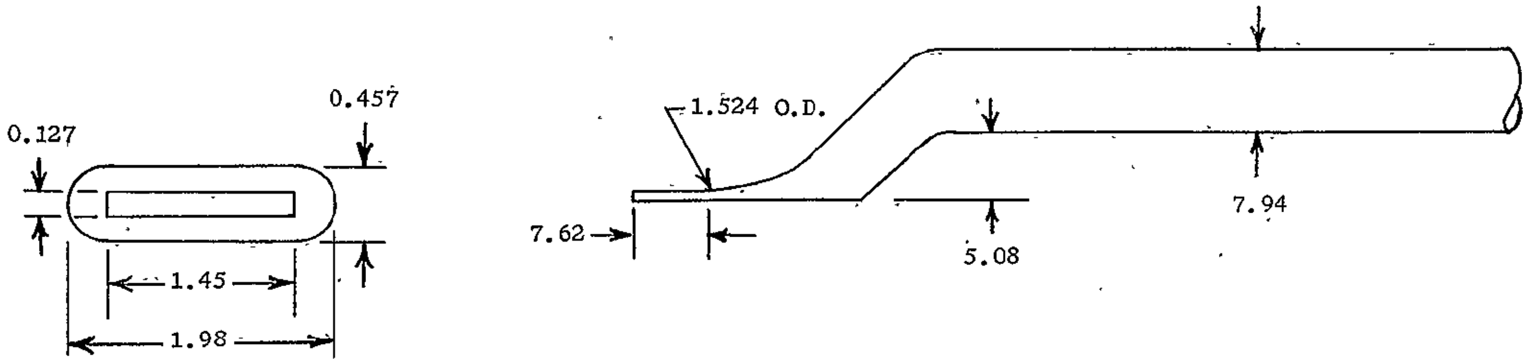

Gas-sampling probe

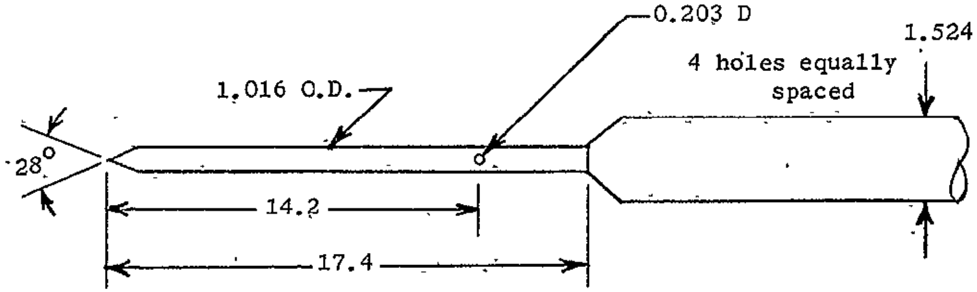

Static-pressure probe

Figure 5.- Survey-probe design. All dimensions in millimeters.

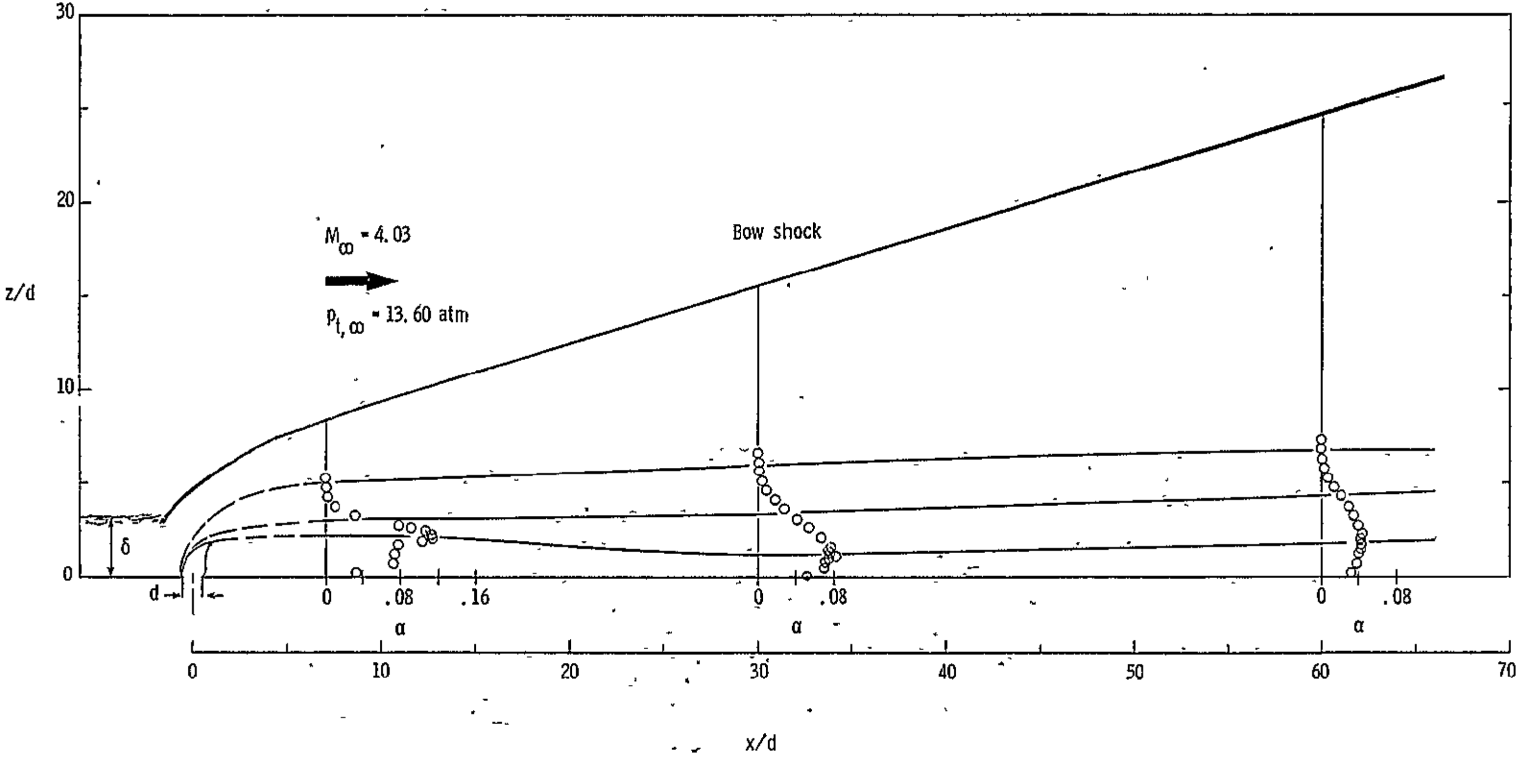

Figure 6.- Structure of flow field and mixing region, $q_r = 1.0$.

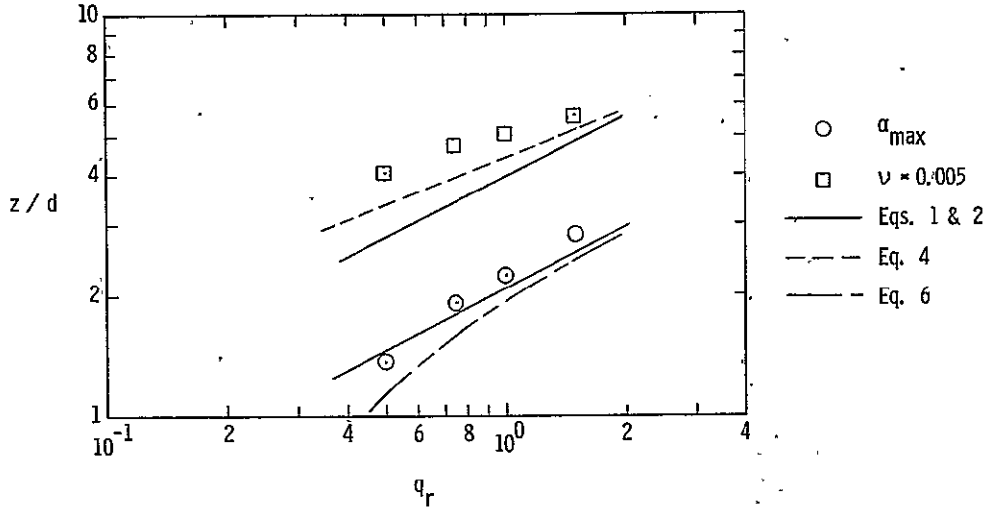

Figure 7.- Effect of dynamic pressure ratio on the jet penetration, $x/d = 7$; comparison of data and correlations.

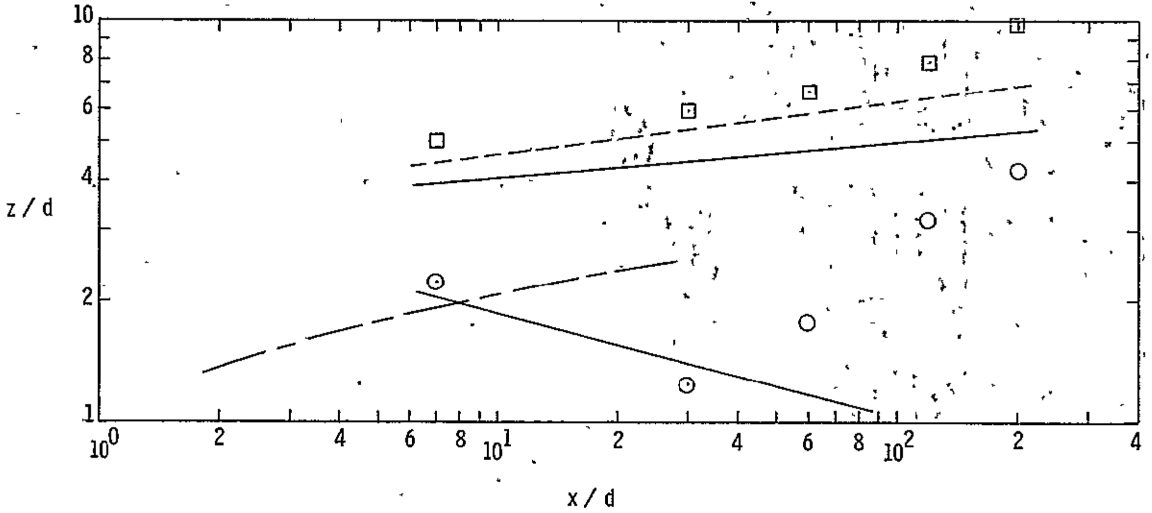

Figure 8.- Maximum concentration and penetration trajectories, $q_r = 1.0$; comparison of data and correlations.

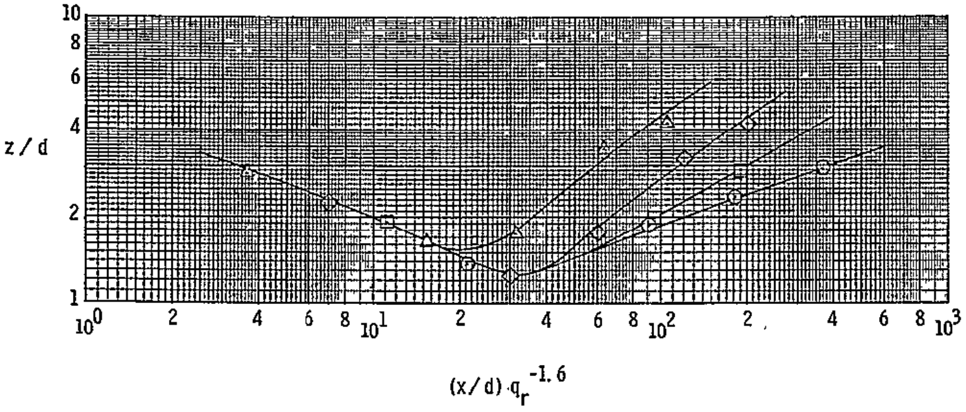

(a) Maximum concentration trajectory.

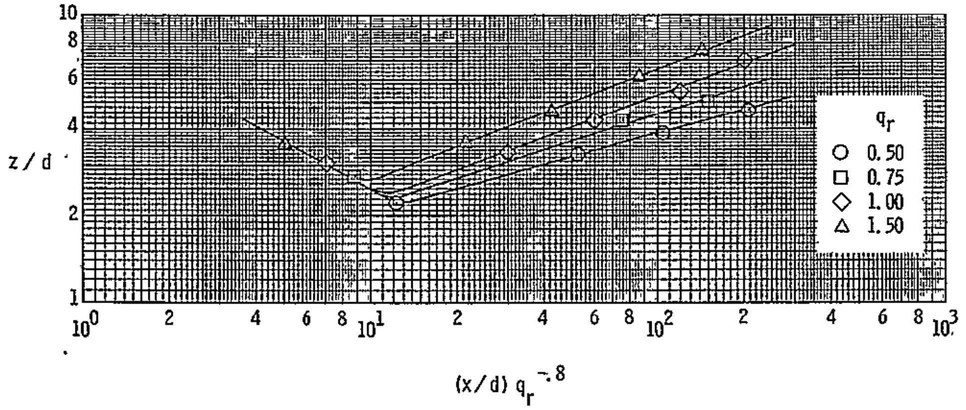

(b) Half-maximum concentration trajectory.

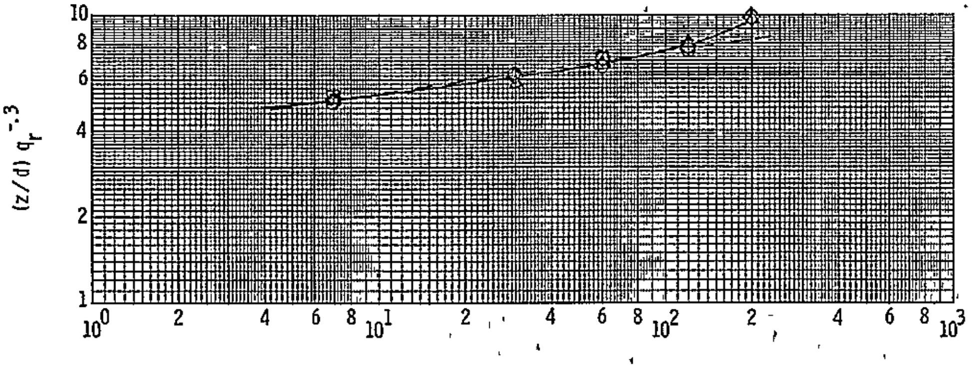

(c) Penetration trajectory, $\nu = 0.005$.

Figure 9.- Effect of dynamic pressure ratio on penetration trajectories.

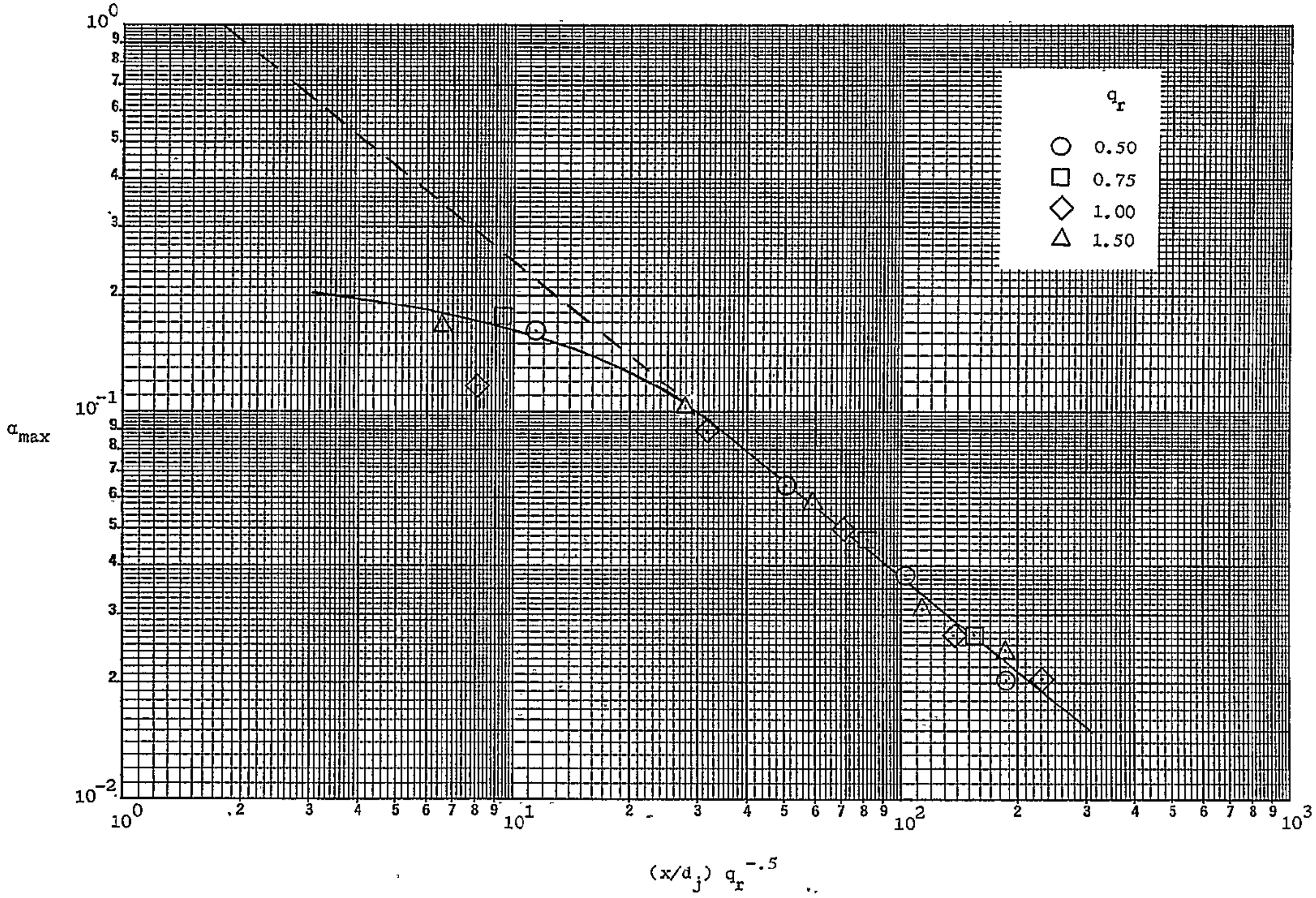

Figure 10.- Decay of maximum concentration.

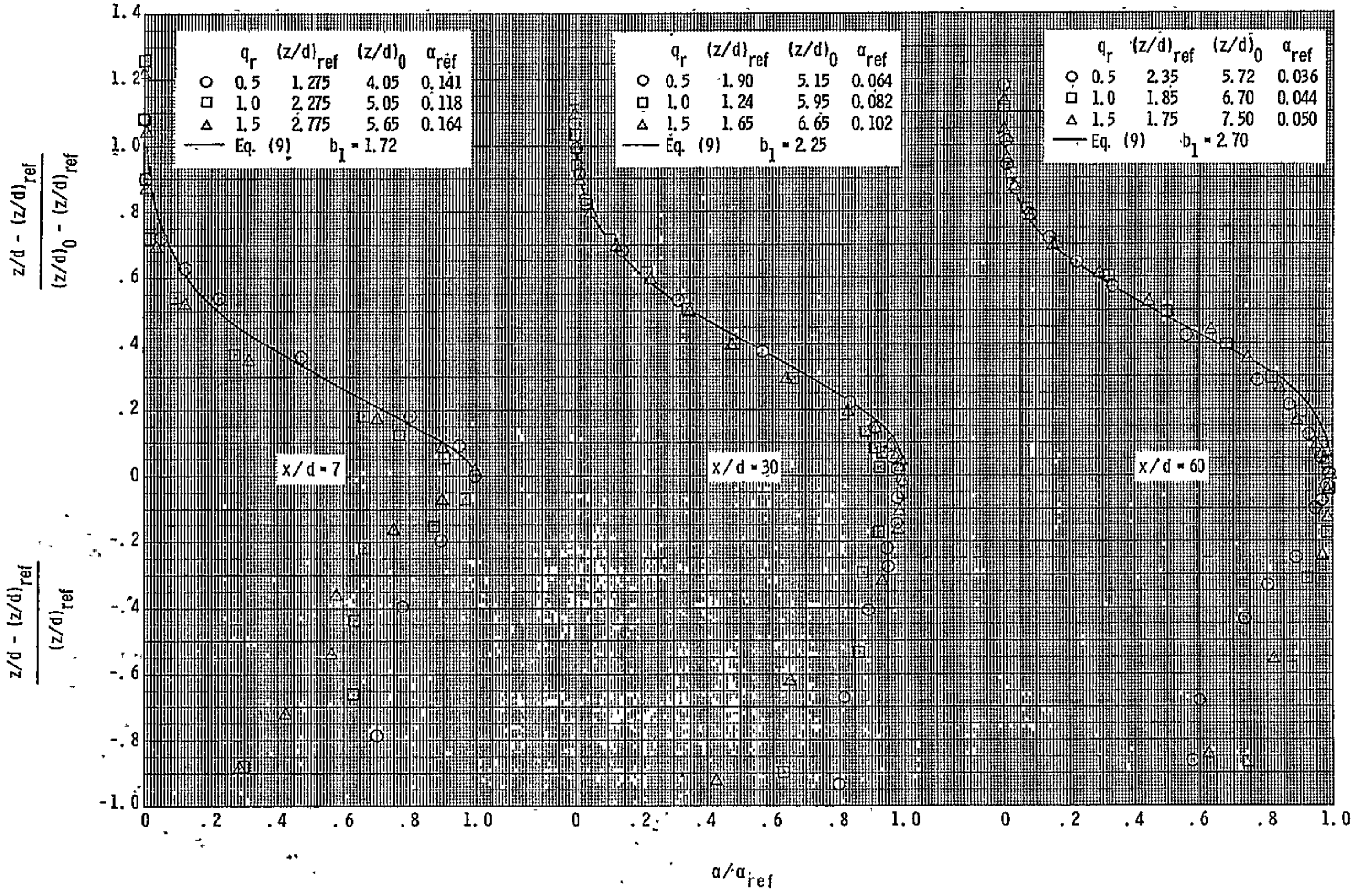

(a) x/d = 7, 30, 60.

Figure 11.- Nondimensional concentration profiles, vertical survey.

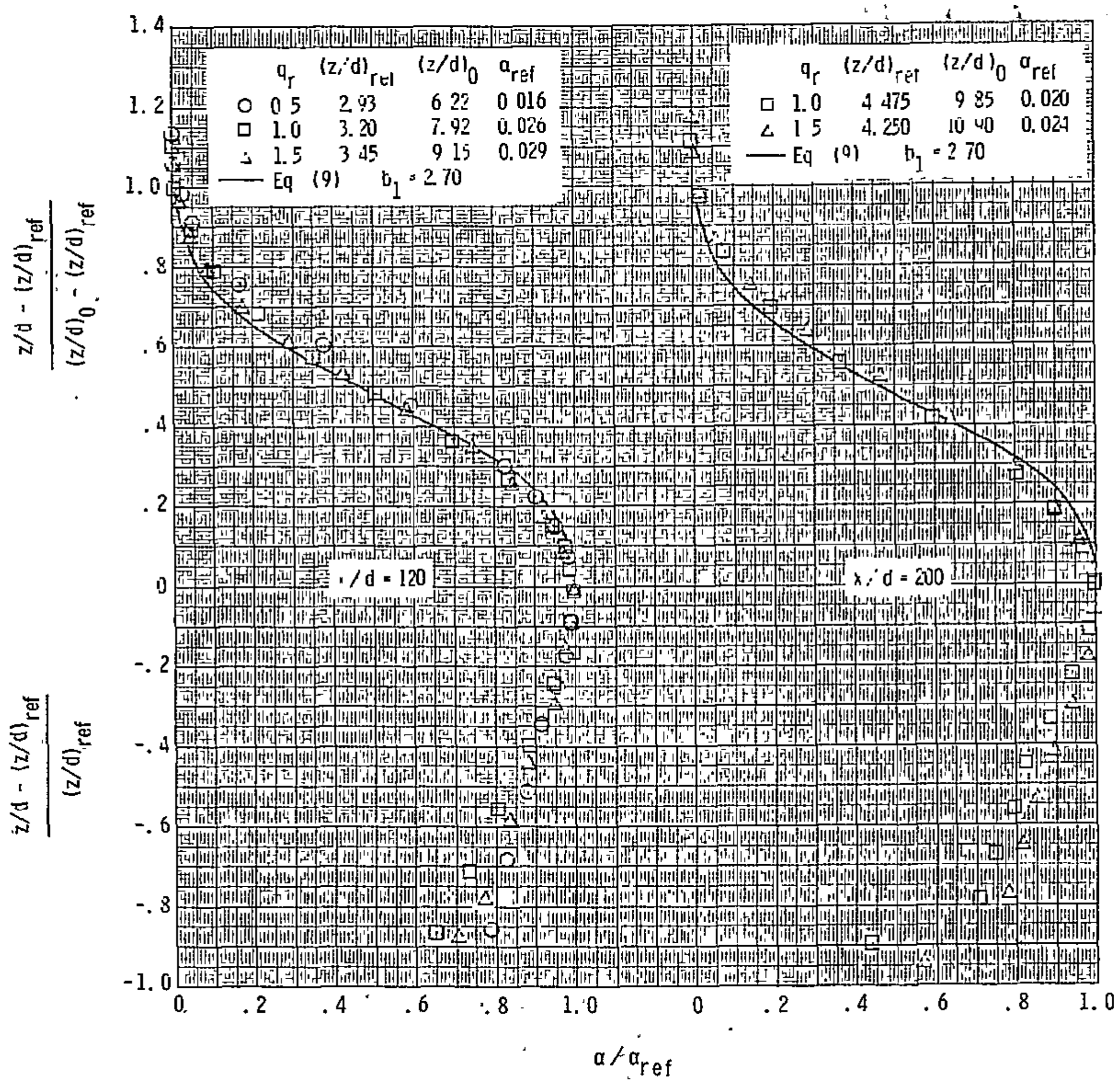

(b) x/d = 120, 200.

Figure 11.- Concluded.

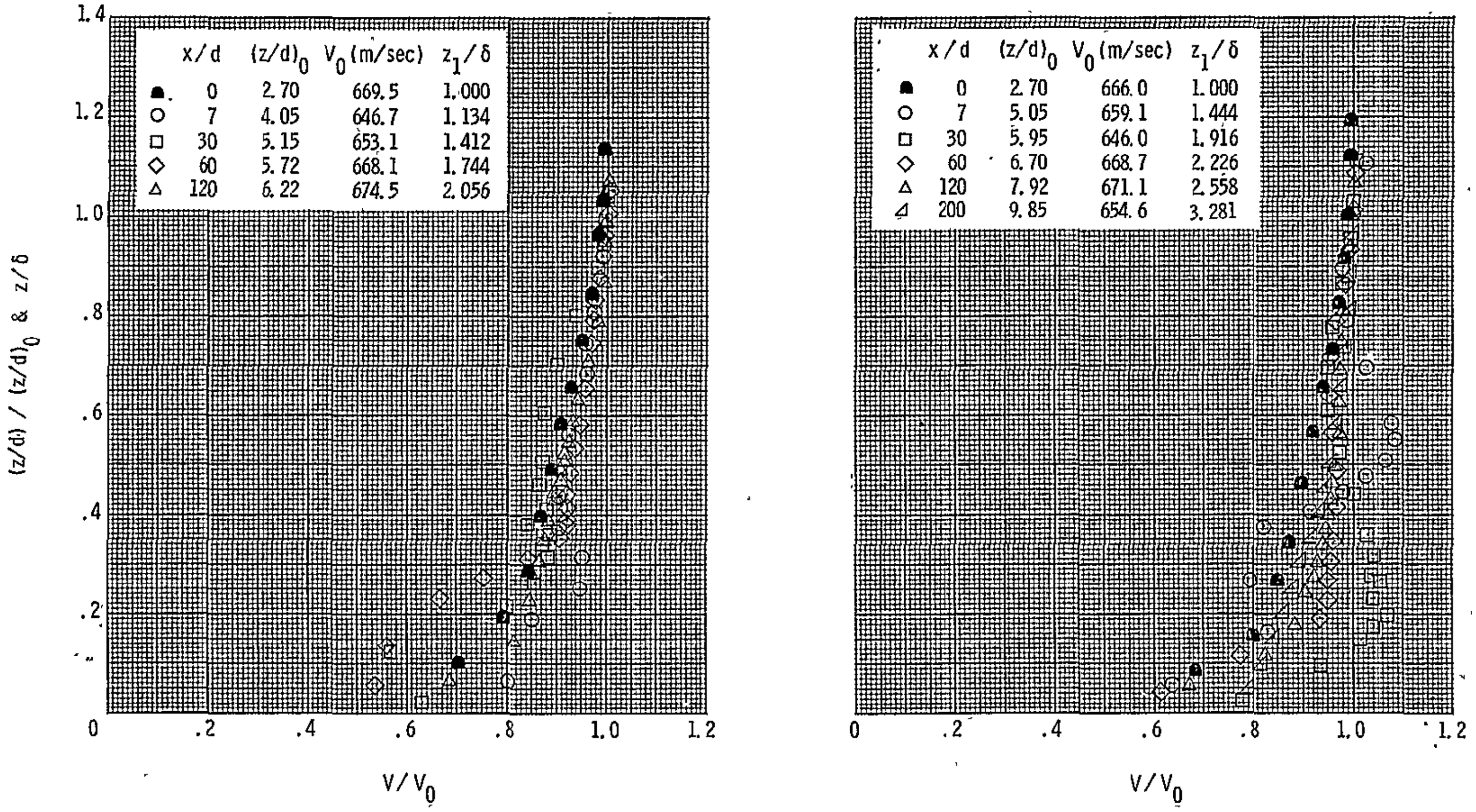

(a) q_r = 0.5.

(b) q_r = 1.0.

Figure 12.- Nondimensional velocity profiles, vertical survey.

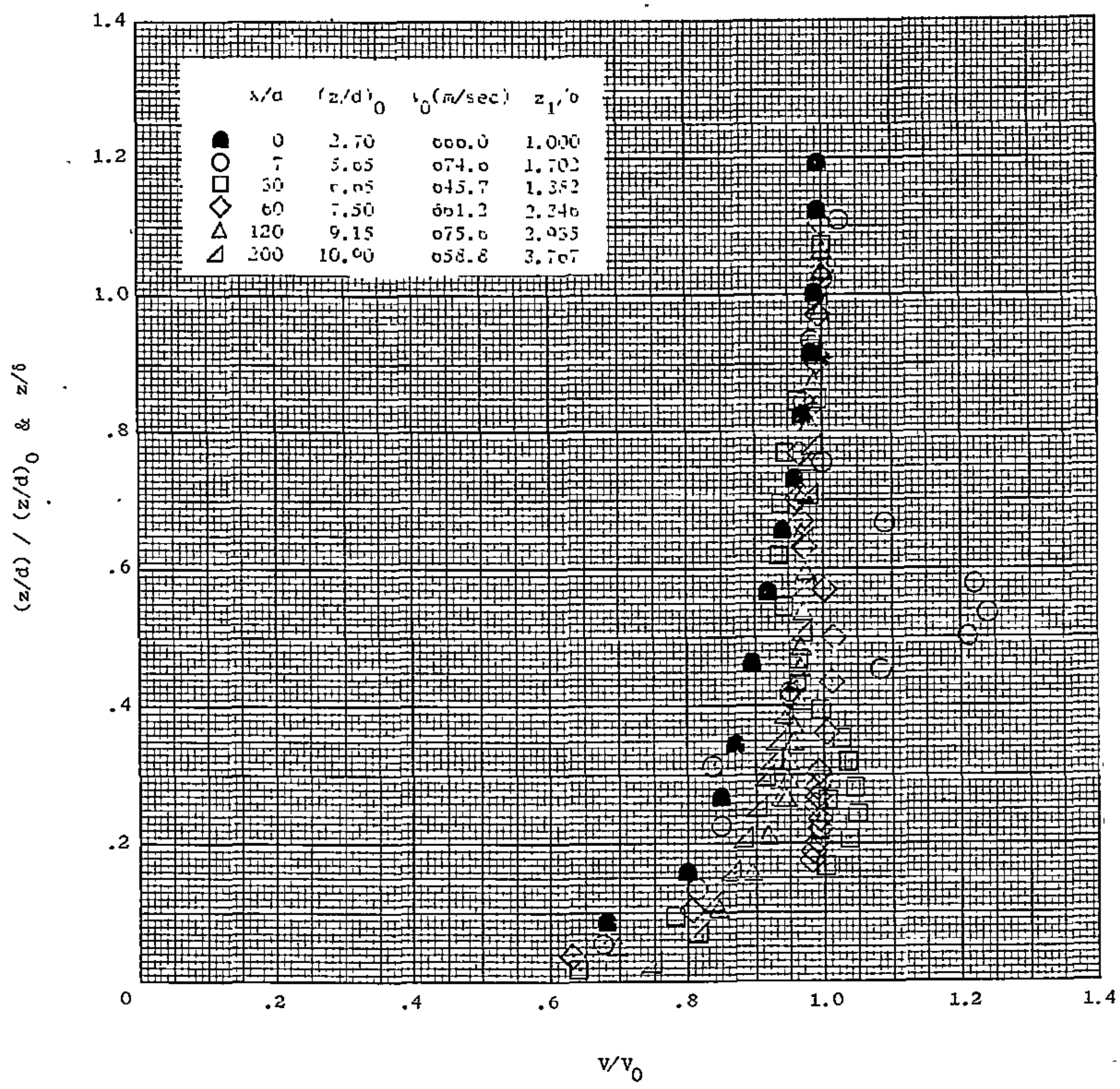

(c) $q_r = 1.5$.

Figure 12.- Concluded.

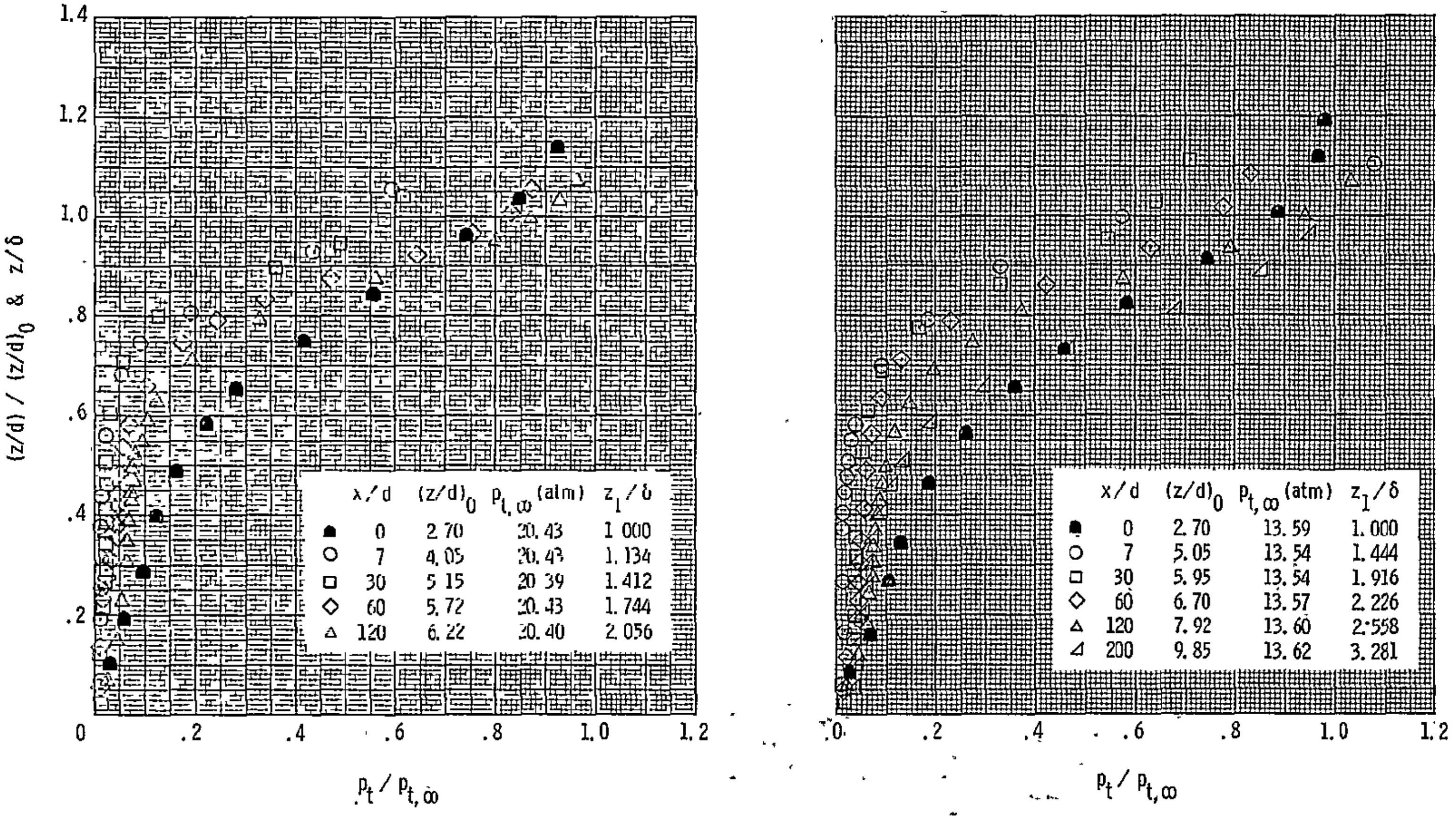

(a) q_r = 0.5.

(b) q_r = 1.0.

Figure 13.- Nondimensional total-pressure profiles, vertical survey.

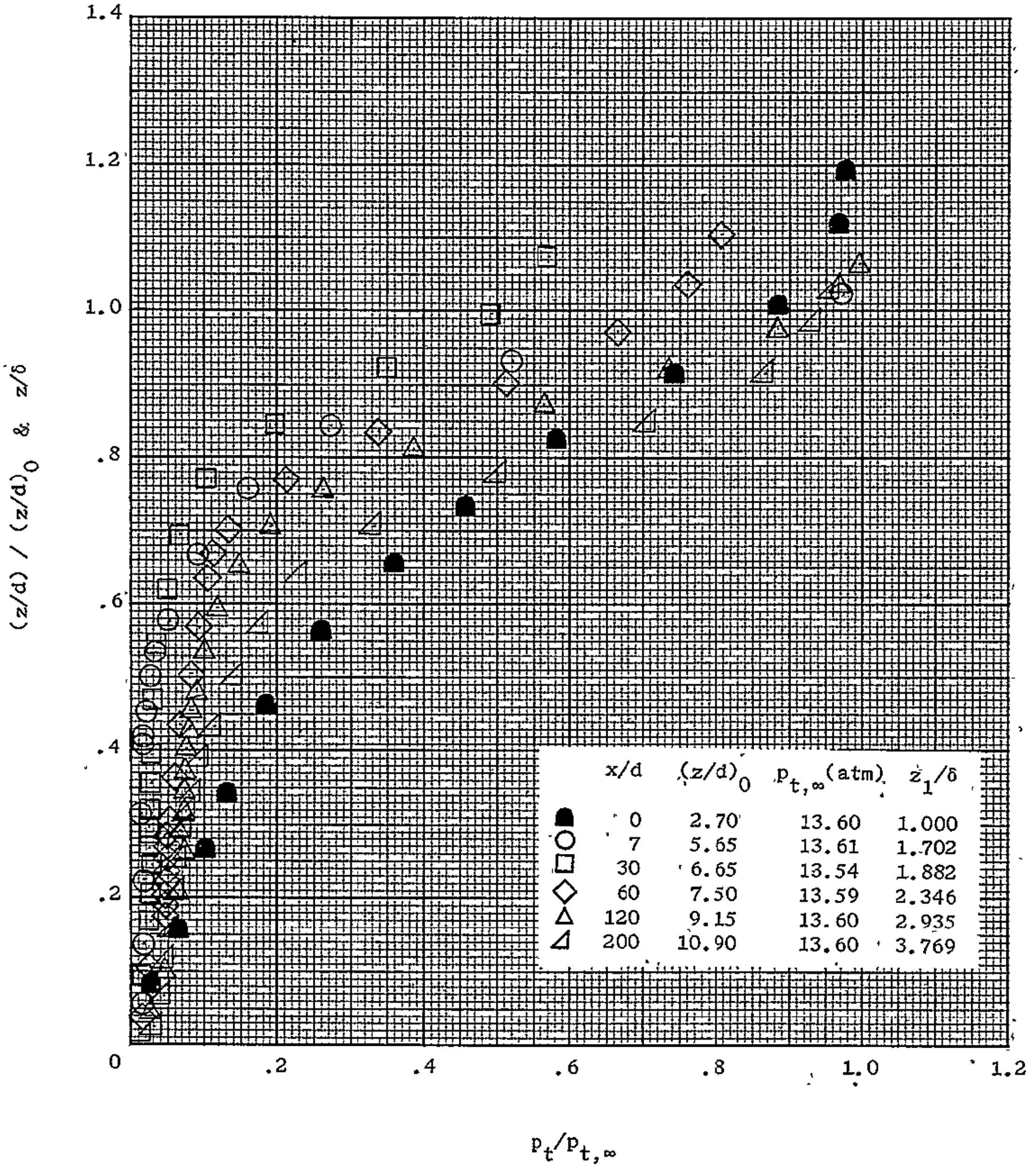

(c) $q_r = 1.5$.

Figure 13.- Concluded.

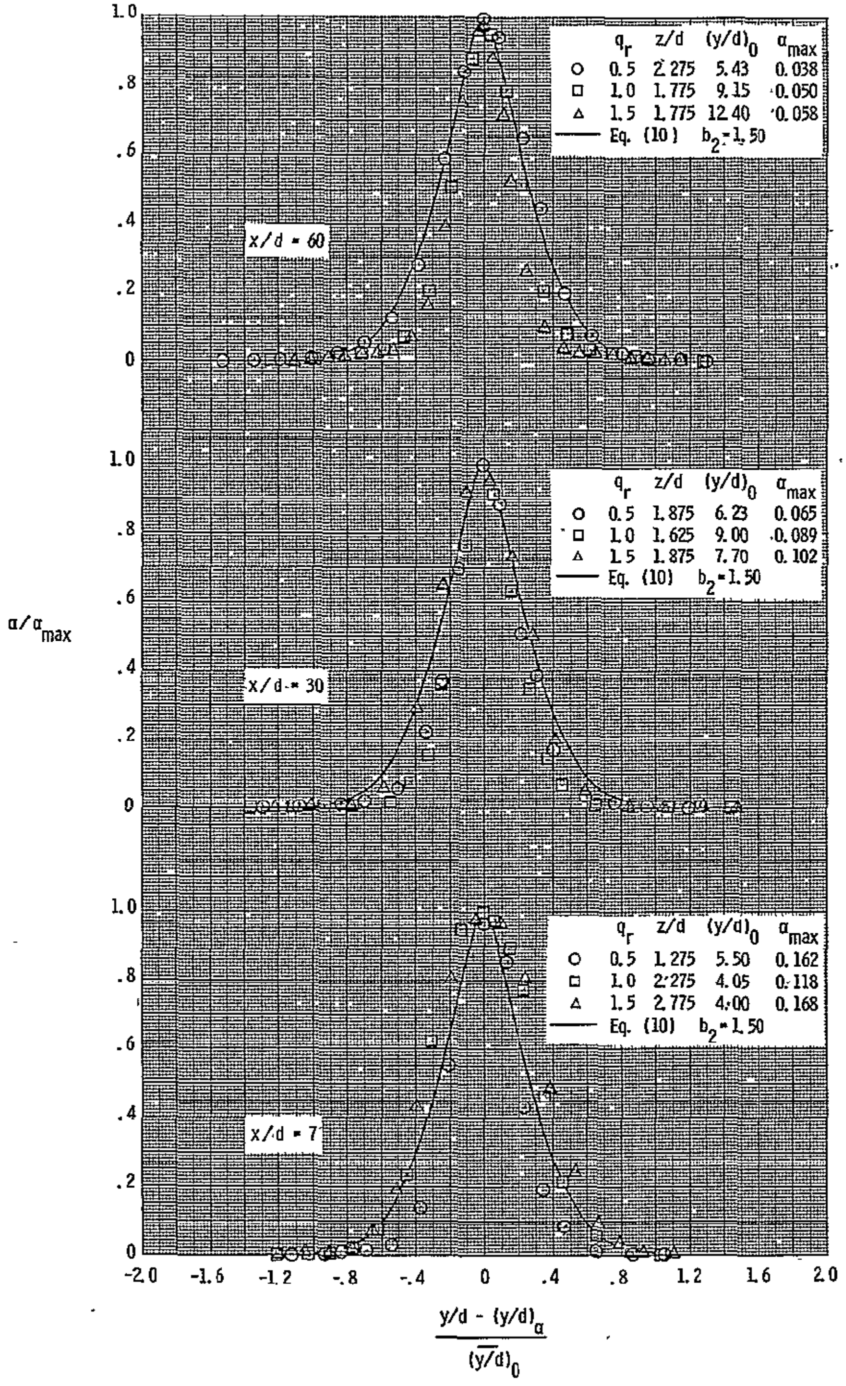

(a) x/d = 7, 30, 60.

Figure 14.- Nondimensional concentration profiles, horizontal survey through point of maximum concentration.

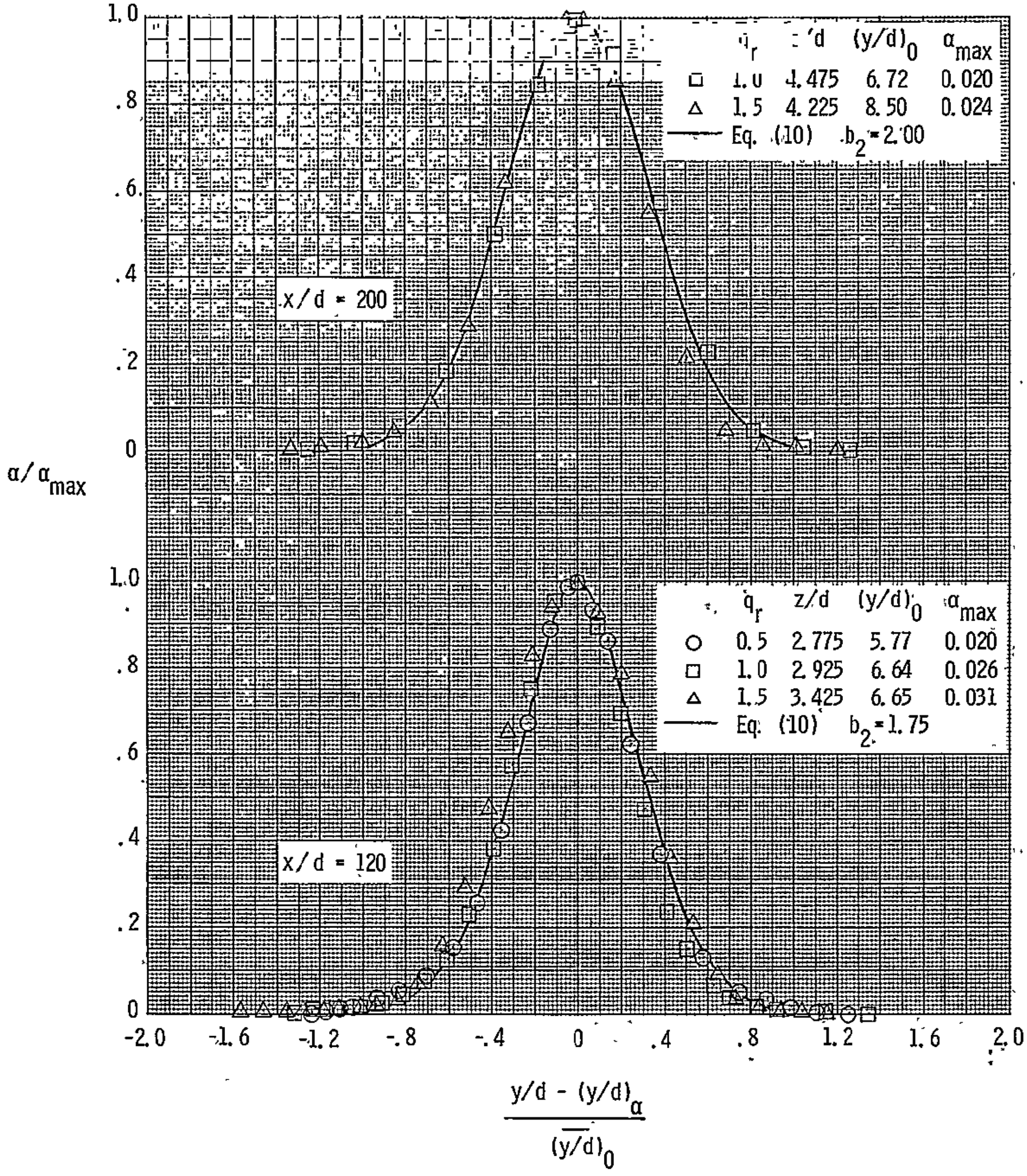

(b) x/d = 120, 200.

Figure 14.- Concluded.

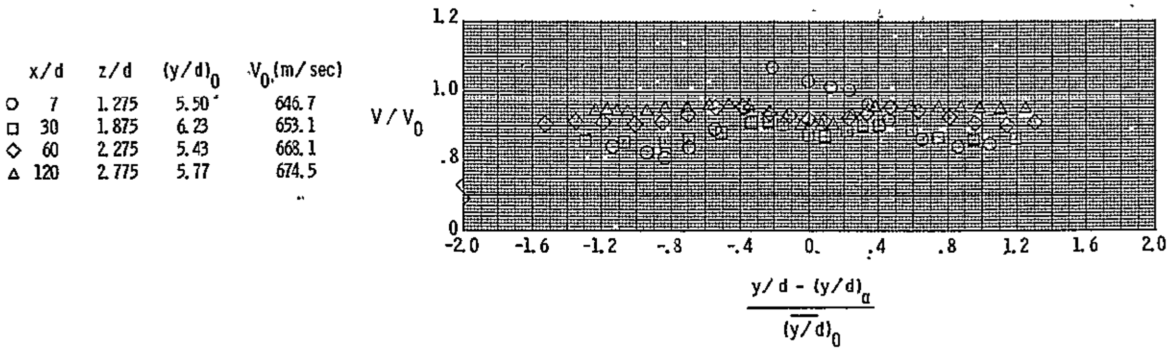

(a) $q_r = 0.5$.

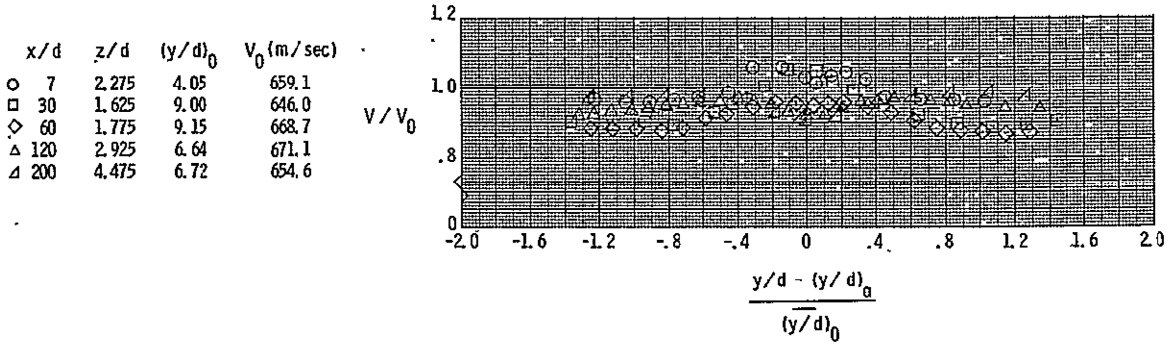

(b) $q_r = 1.0$.

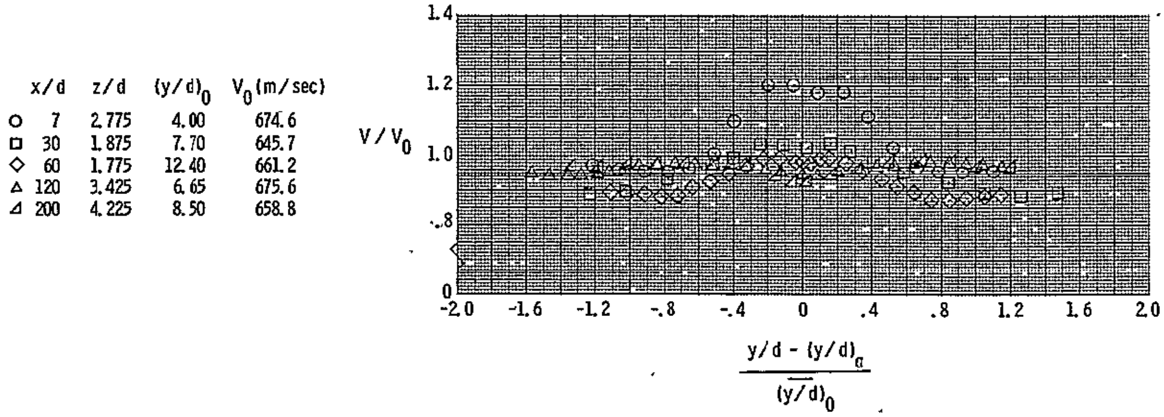

(c) $q_r = 1.5$.

Figure 15.- Nondimensional velocity profiles, horizontal survey through point of maximum concentration.

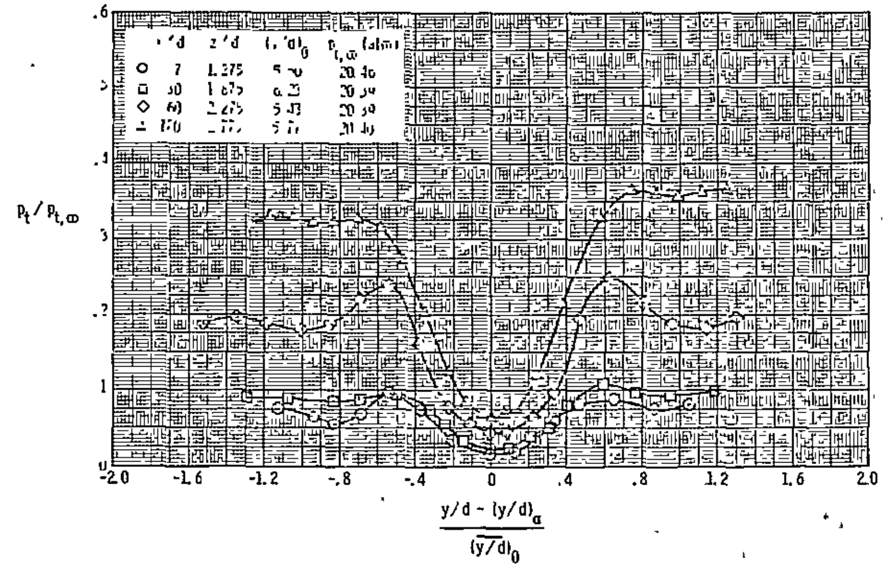

(a) $q_r = 0.5$.

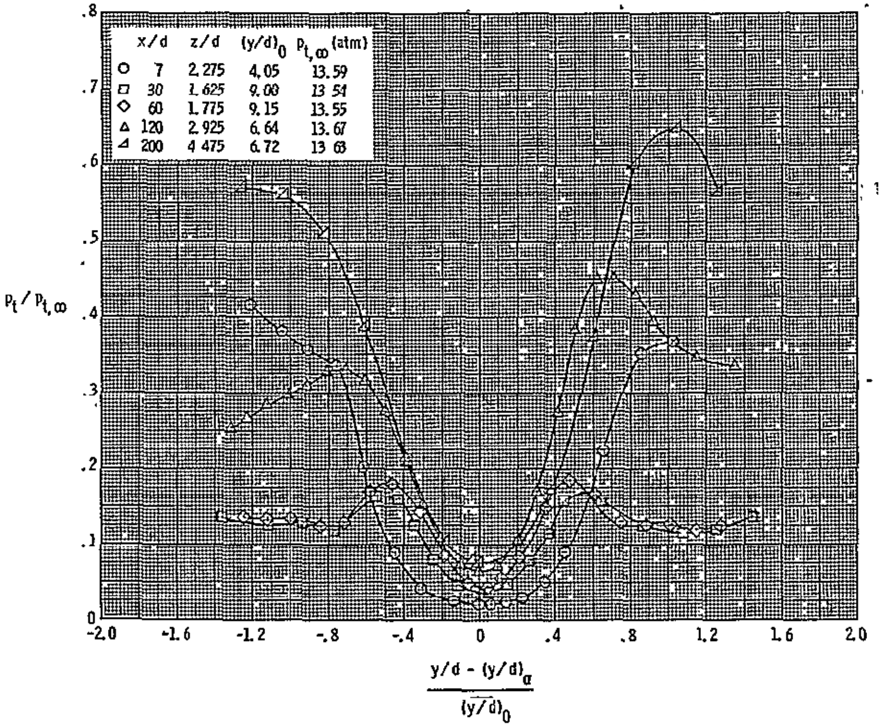

(b) $q_r = 1.0$.

Figure 16.- Nondimensional total pressure profiles, horizontal survey through point of maximum concentration.

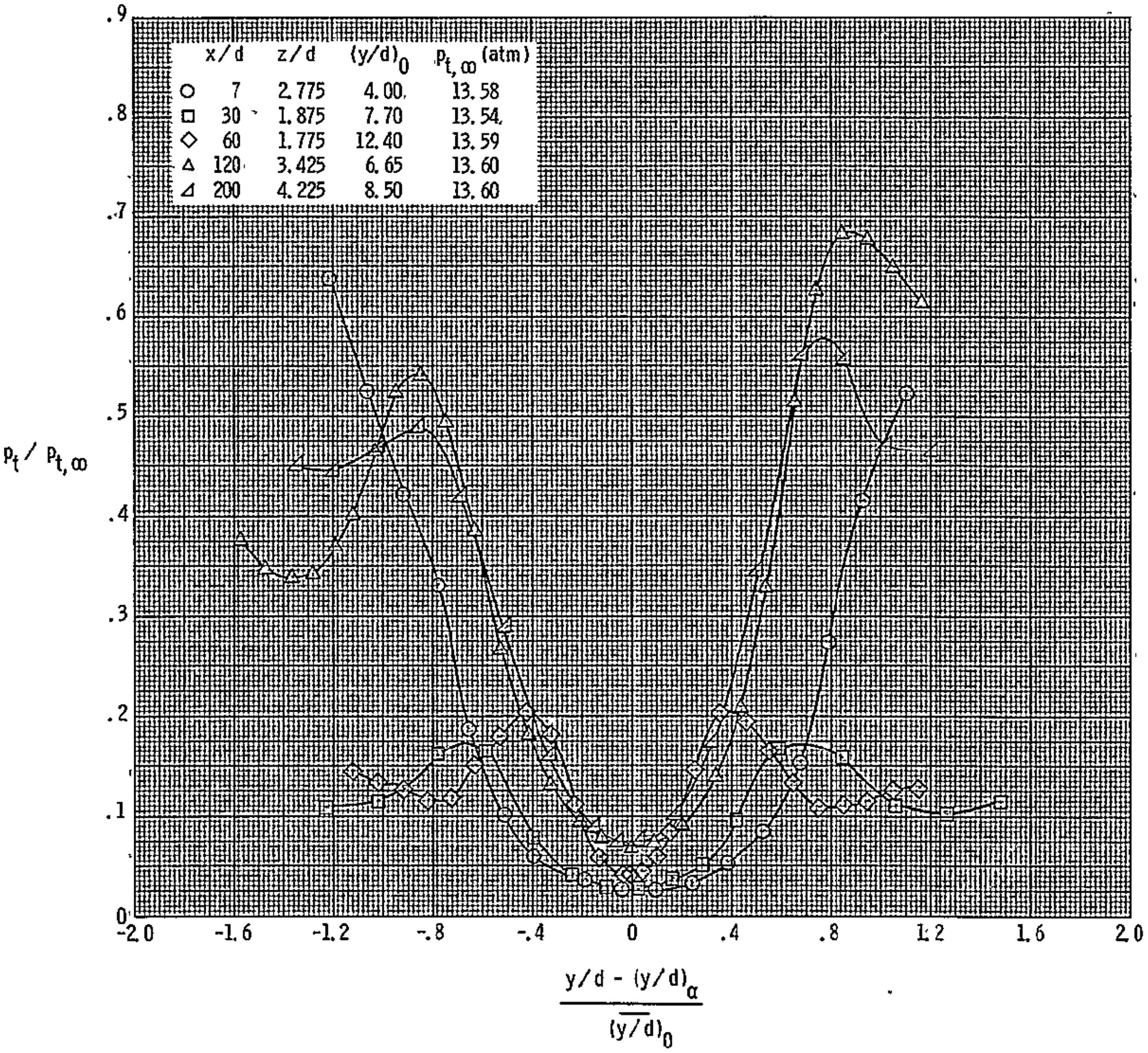

(c) $q_r = 1.5$.

Figure 16.- Concluded.

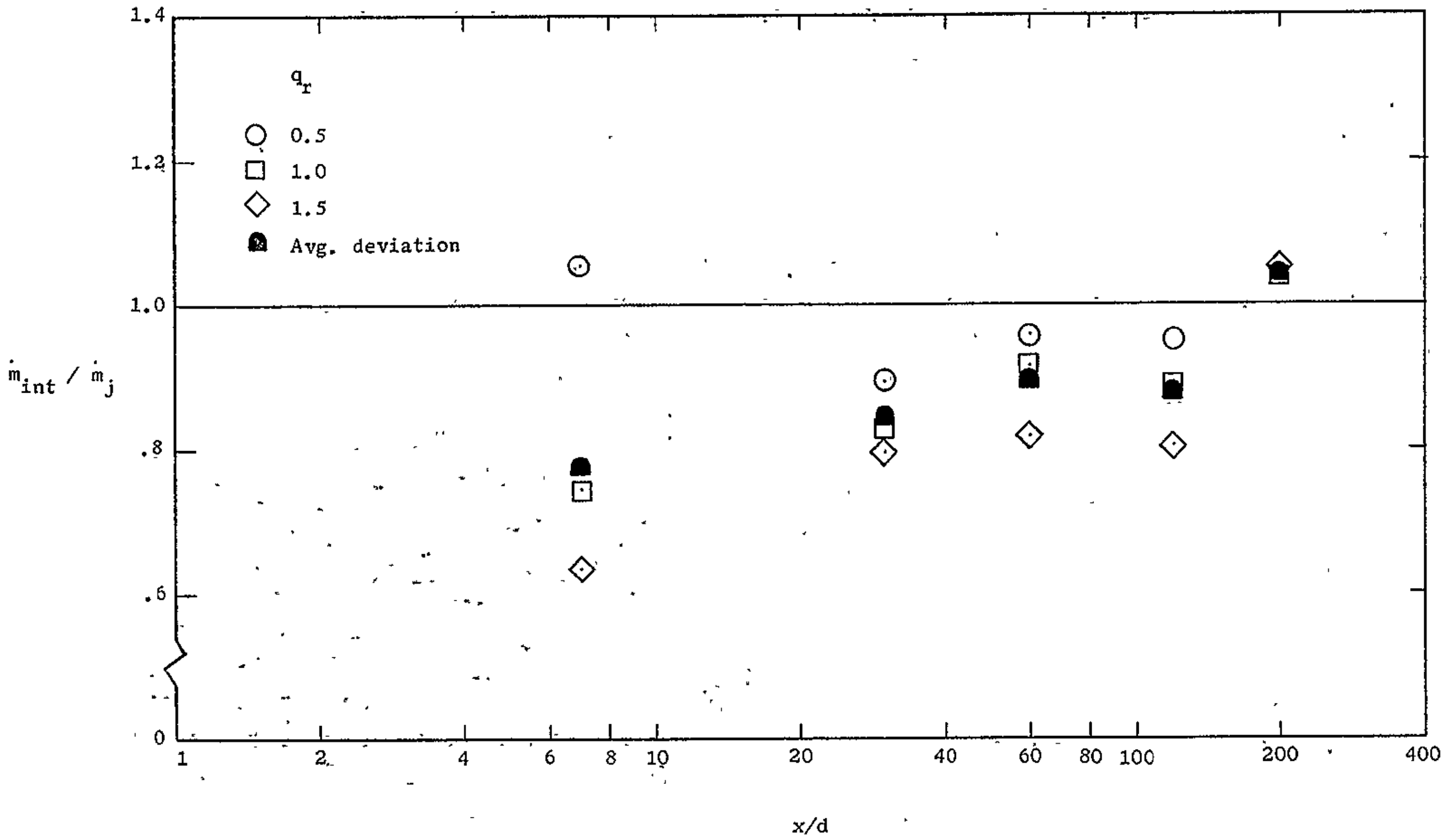

Figure 17.- Results of fuel mass flow contour integration.

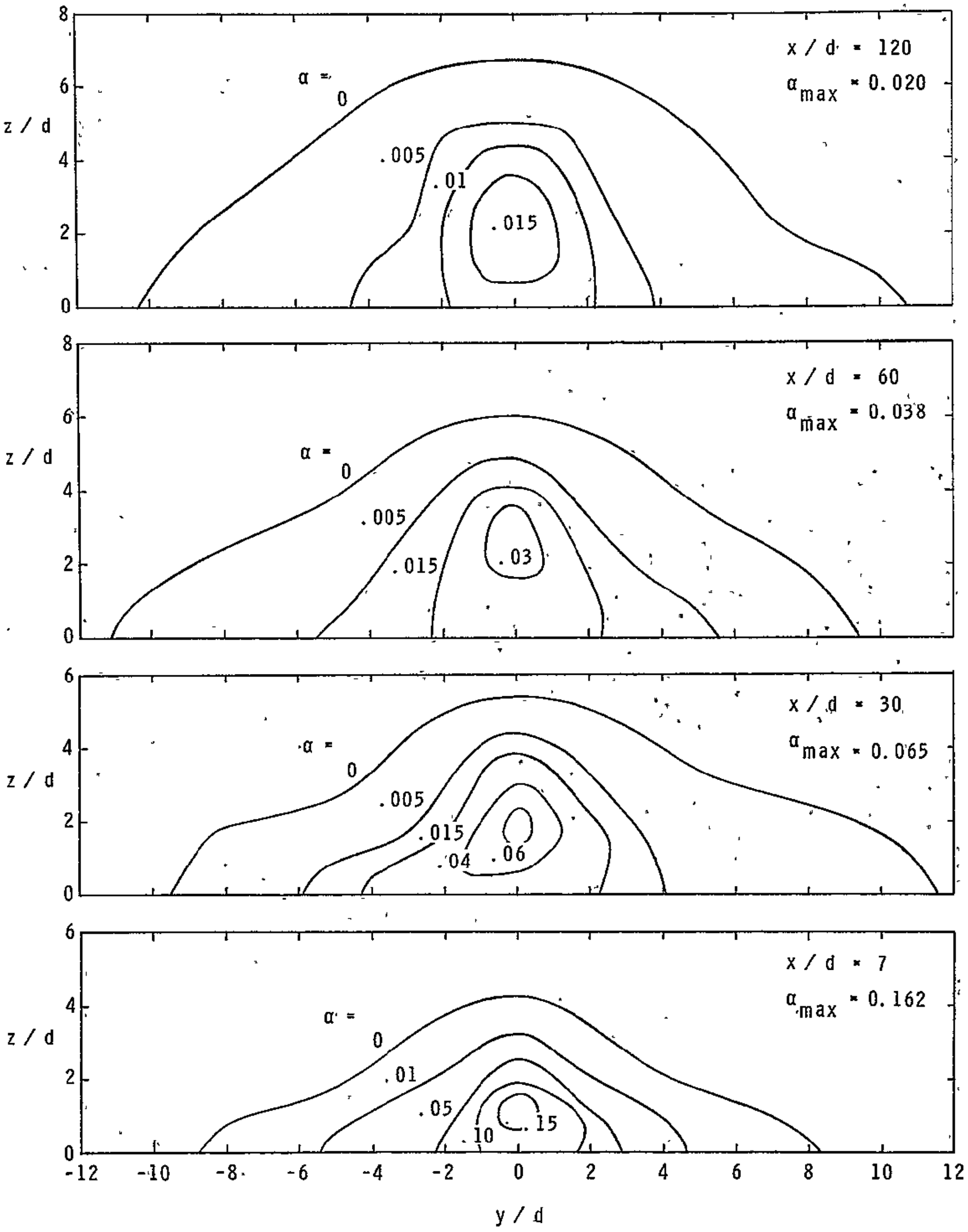

(a) $q_r = 0.5$.

Figure 18.- Hydrogen mass fraction contours.

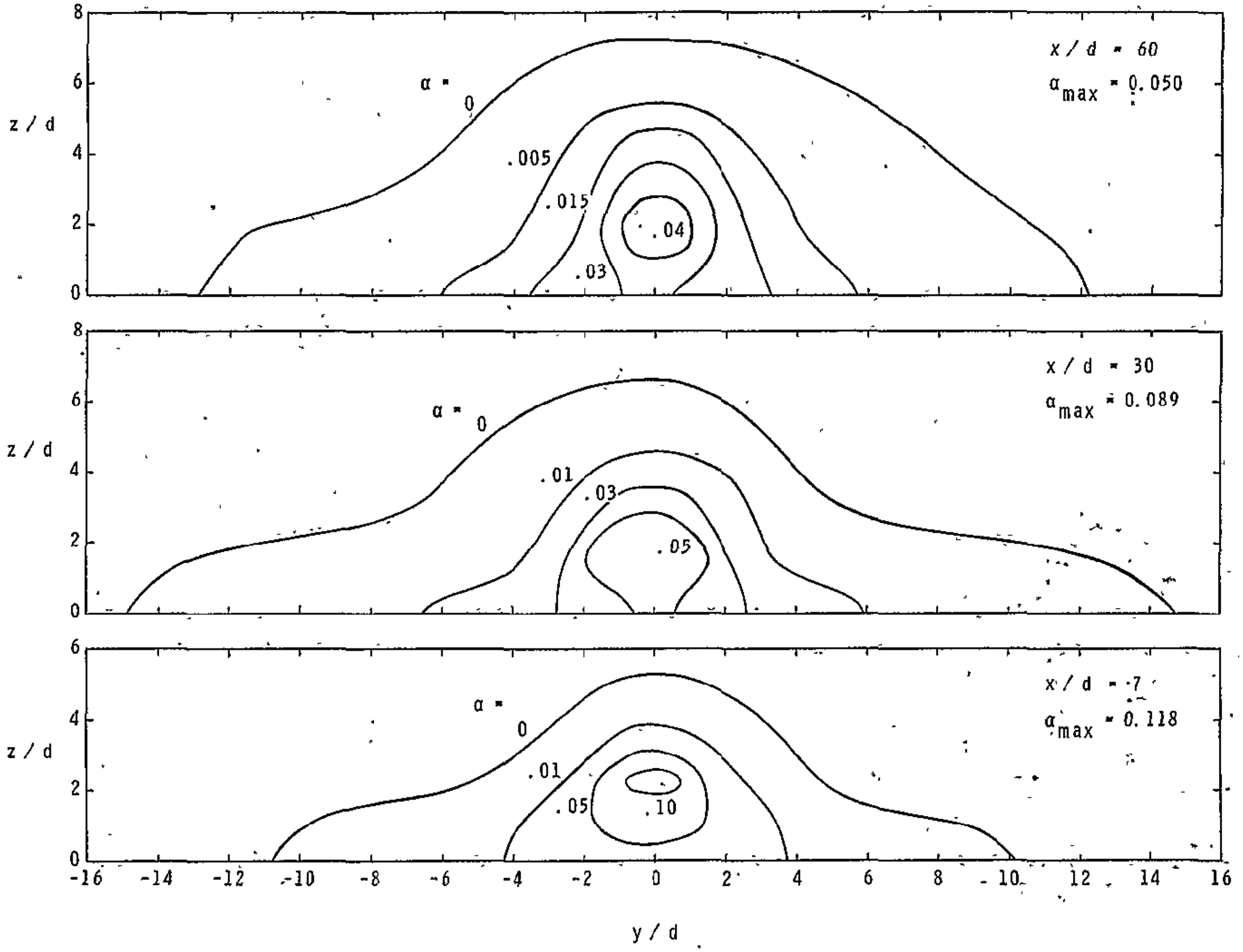

(b) $q_r = 1.0$.

Figure 18.- Continued.

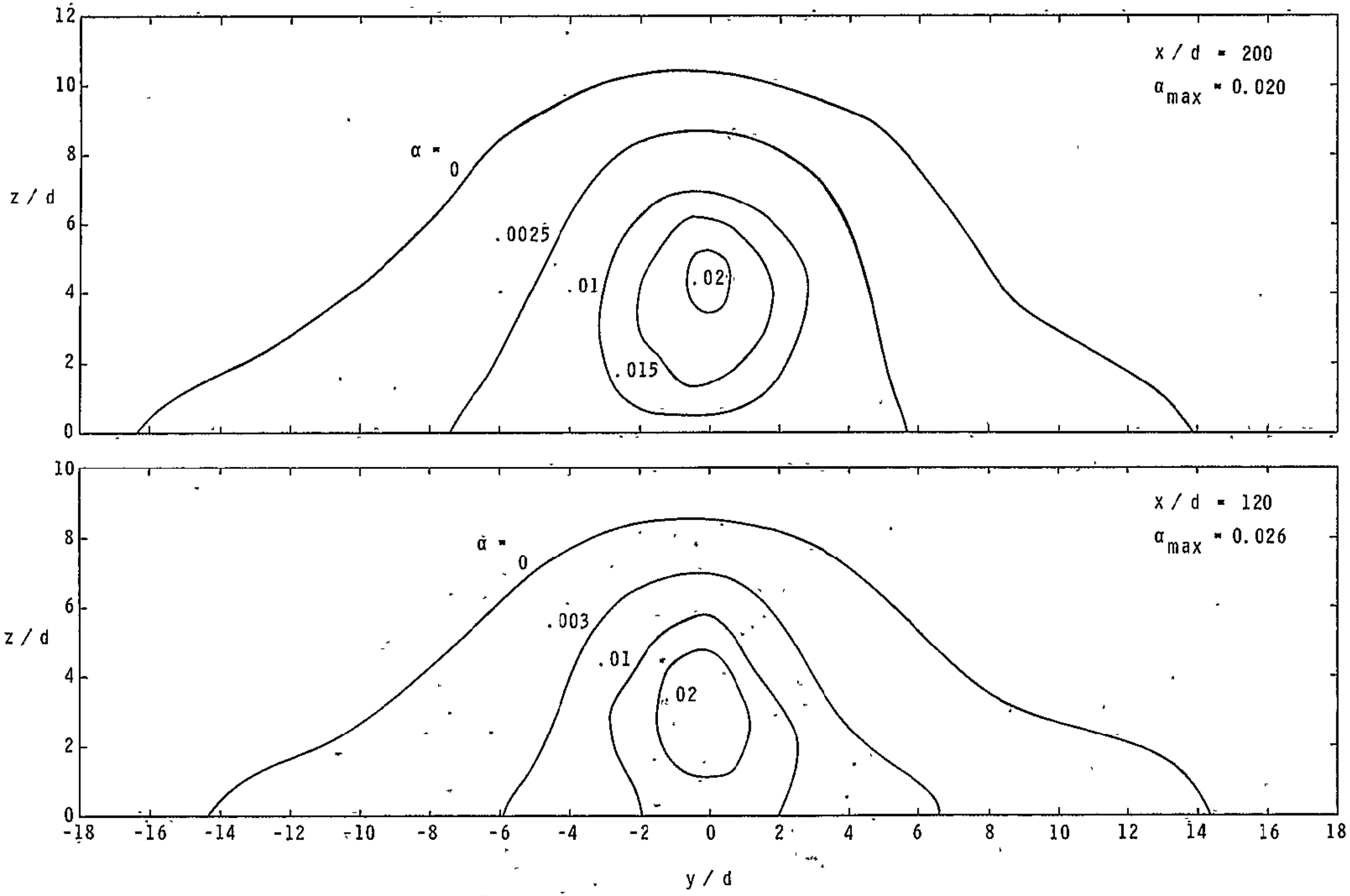

(b) q_r = 1.0 (concluded).

Figure 18.- Continued.

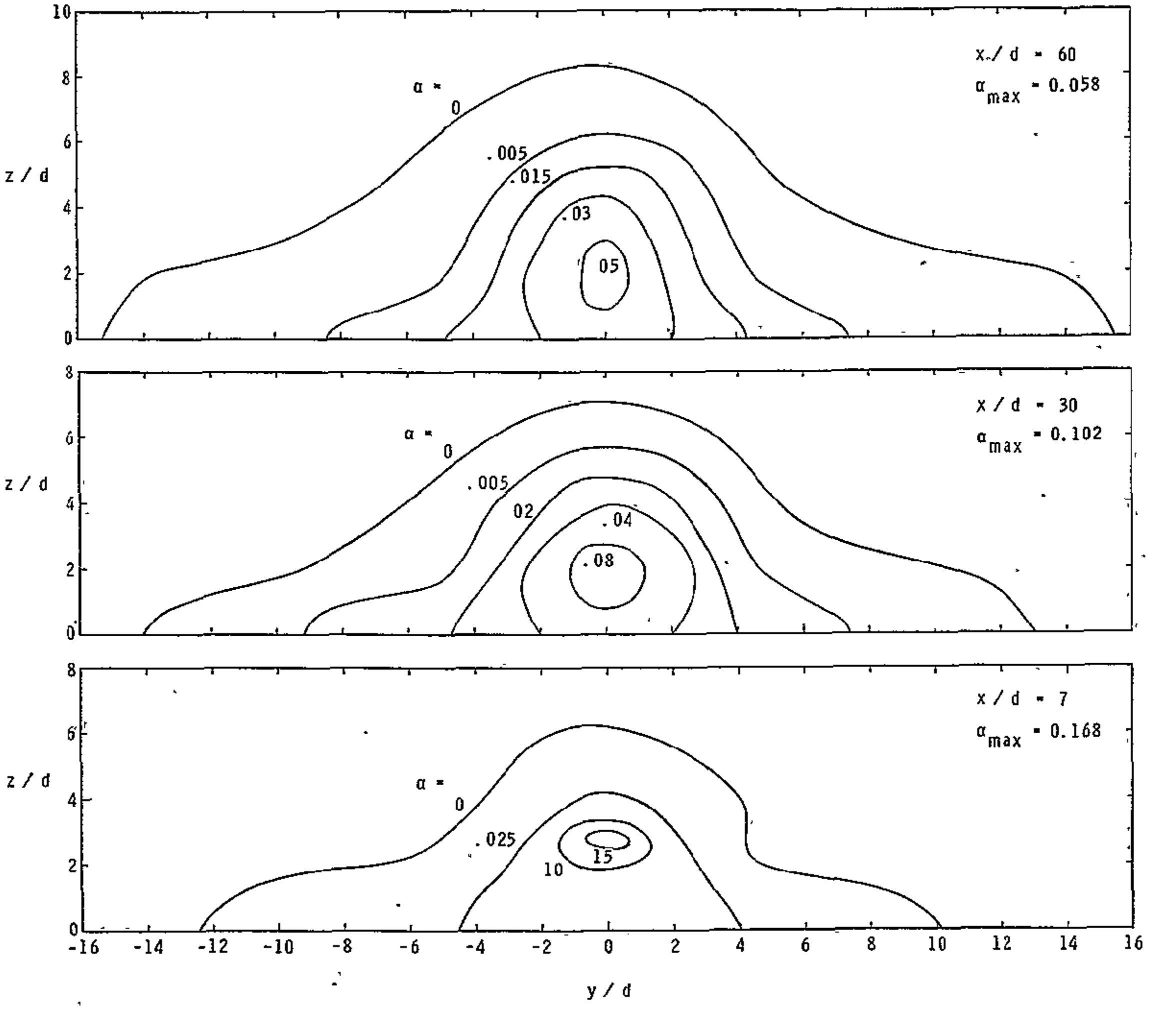

(c) $q_r = 1.5$.

Figure 18.- Continued.

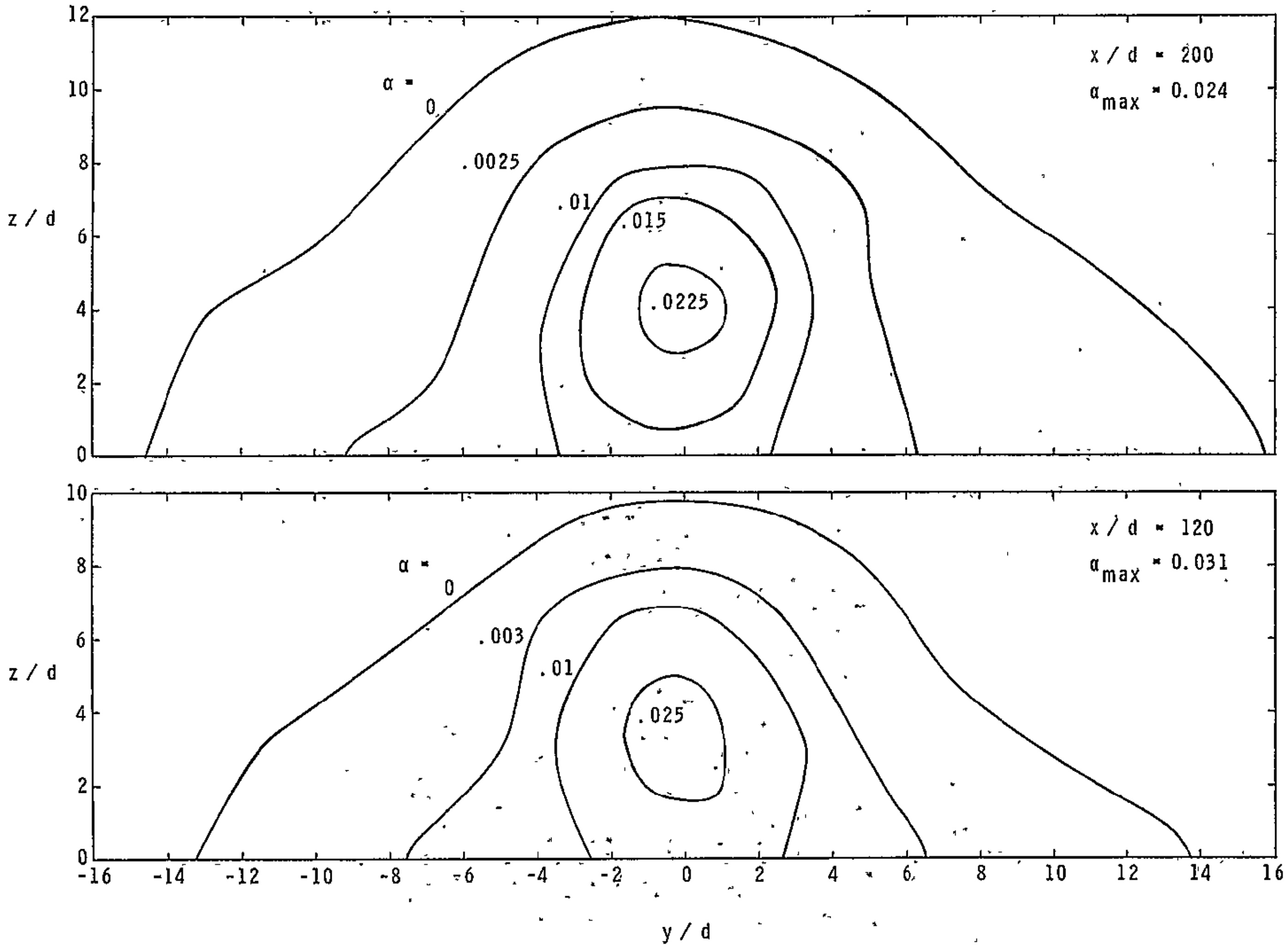

(c) $q_r = 1.5$ (concluded).

Figure 18.- Concluded.

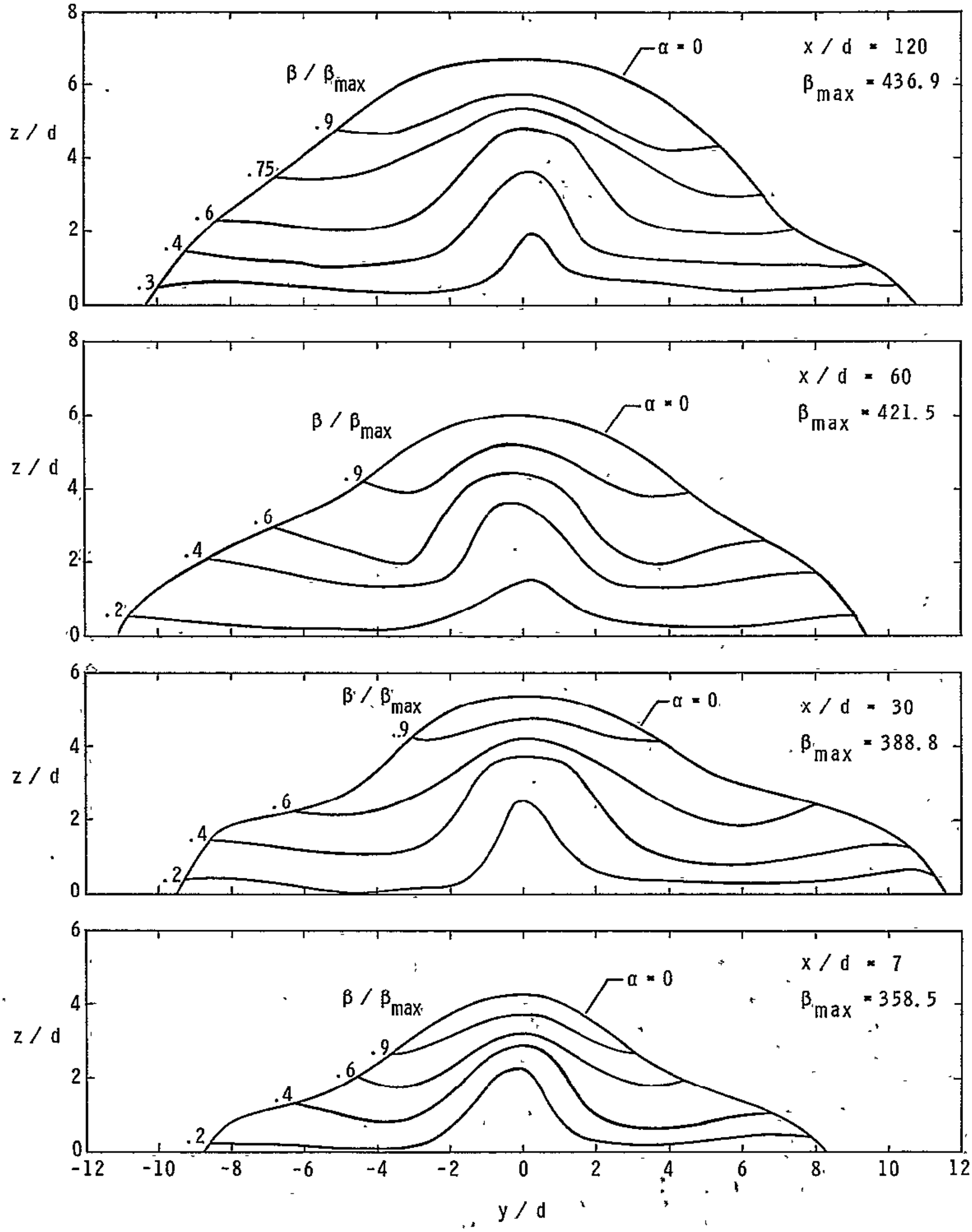

(a) $q_r = 0.5$.

Figure 19.- Air mass flow contours.

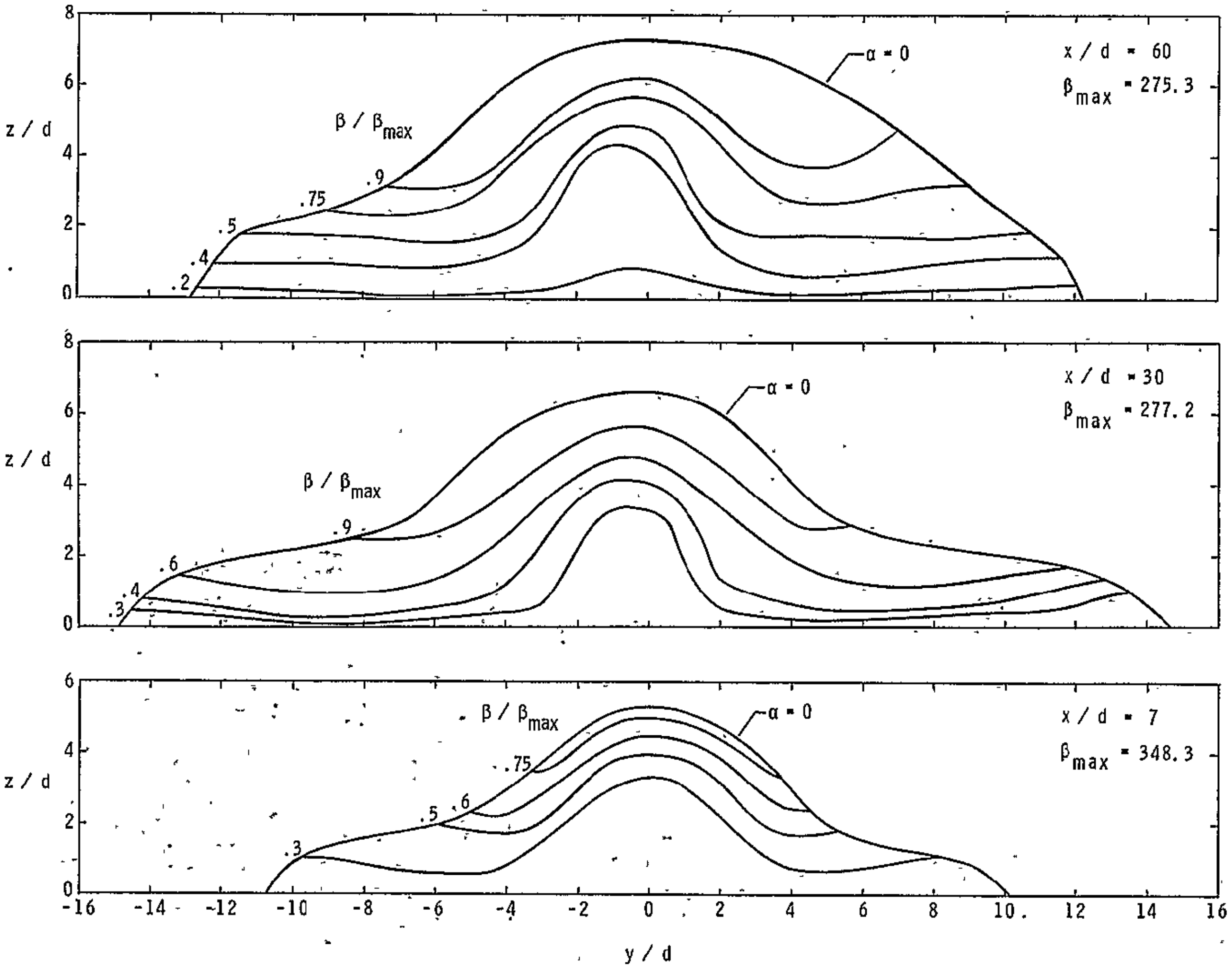

(b) $q_r = 1.0$.

Figure 19.- Continued.

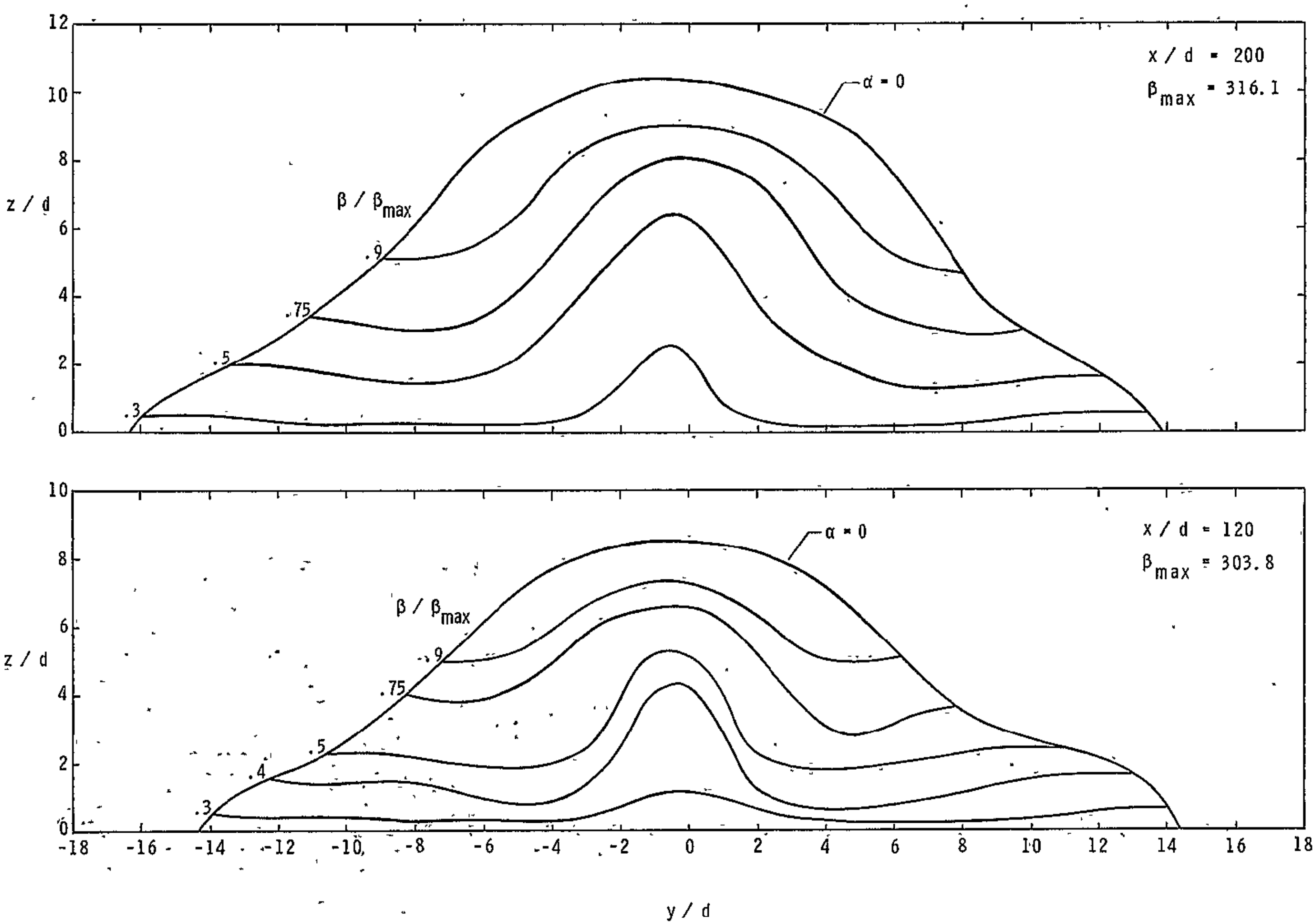

(b) q_r = 1.0 (concluded).

Figure 19.- Continued.

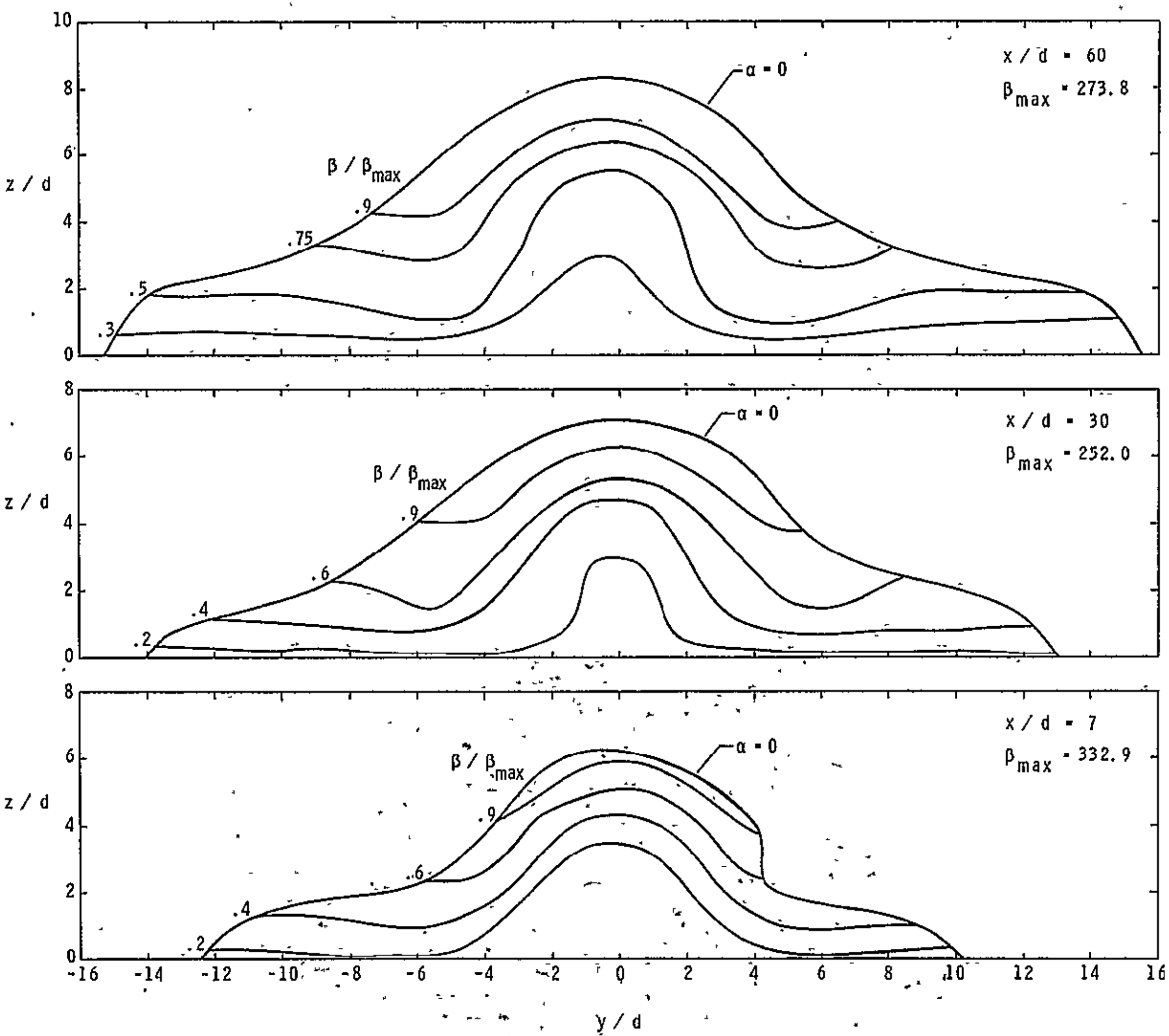

(c) $q_r = 1.5$.

Figure 19.- Continued.

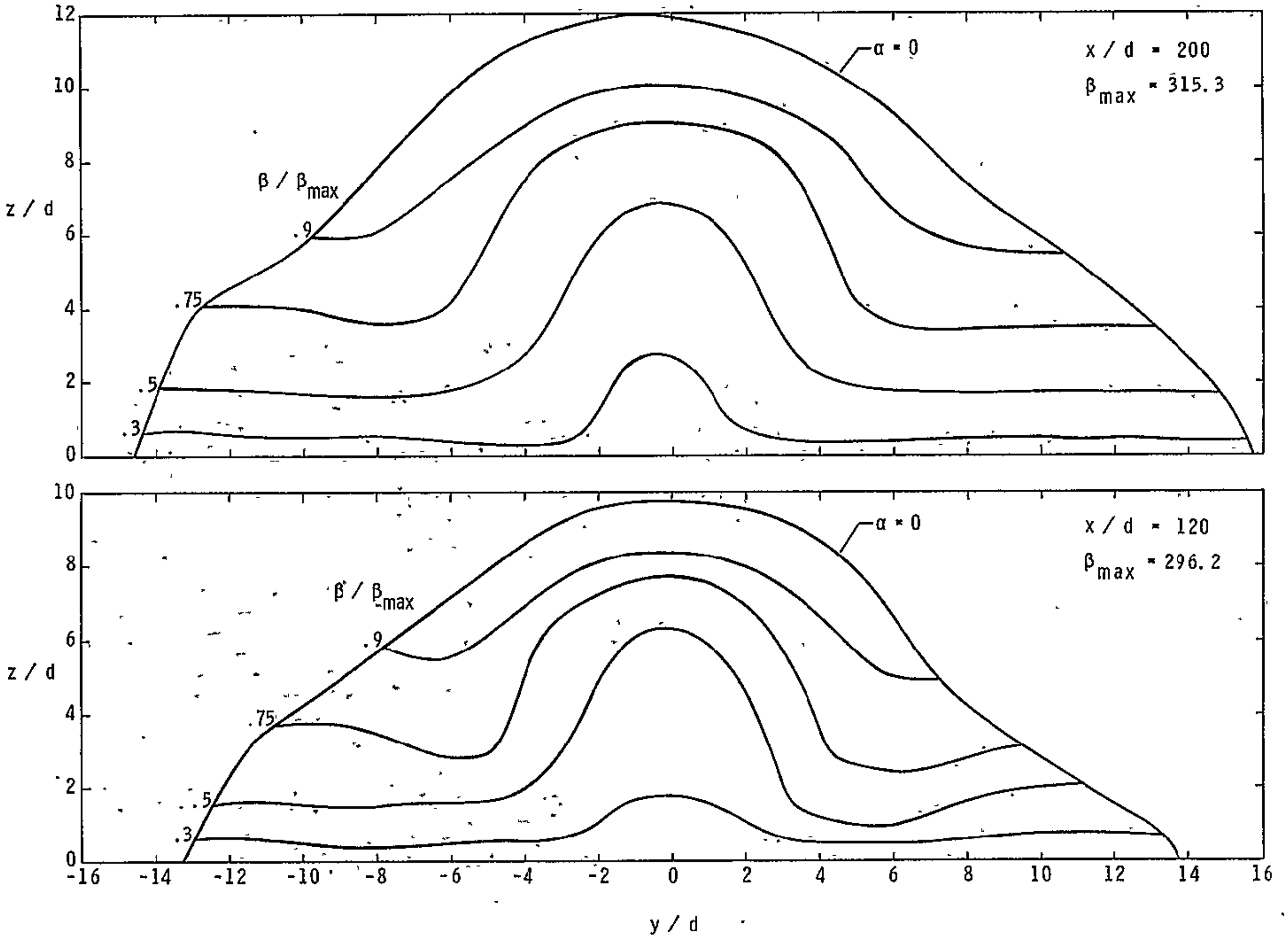

(c) q_r = 1.5 (concluded).

Figure 19.- Concluded.

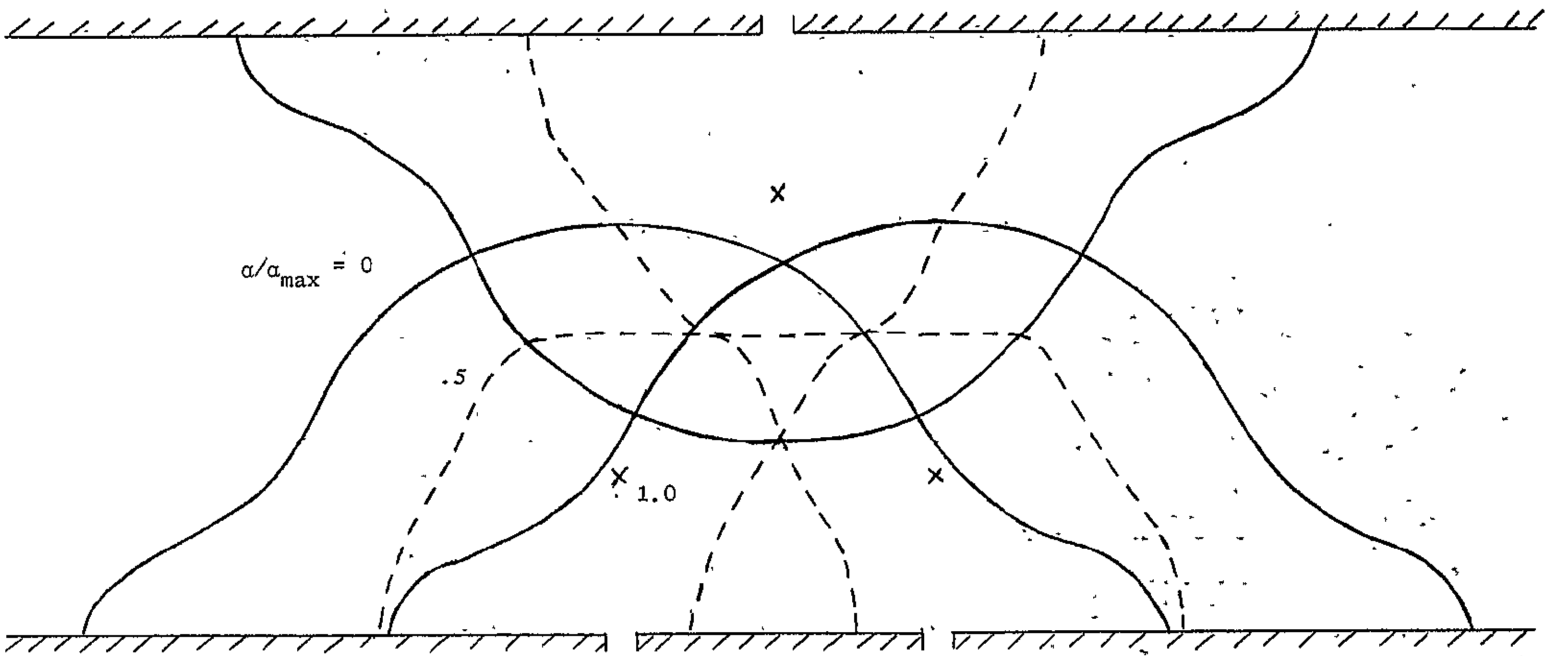

Figure 20.- Schematic of flow field cross section for opposite staggered injection by superposition of single jet contours.

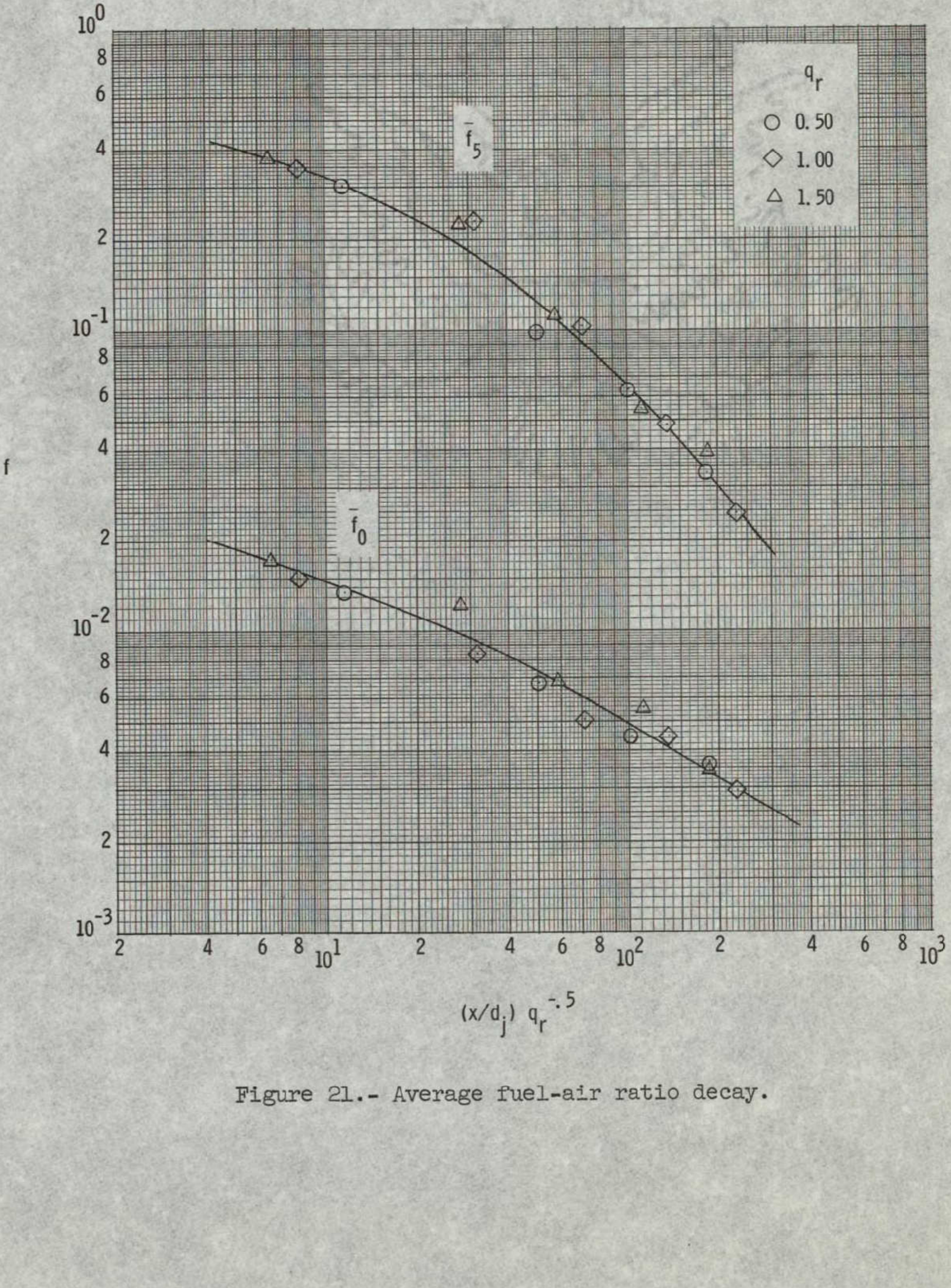

Figure 21.- Average fuel-air ratio decay.

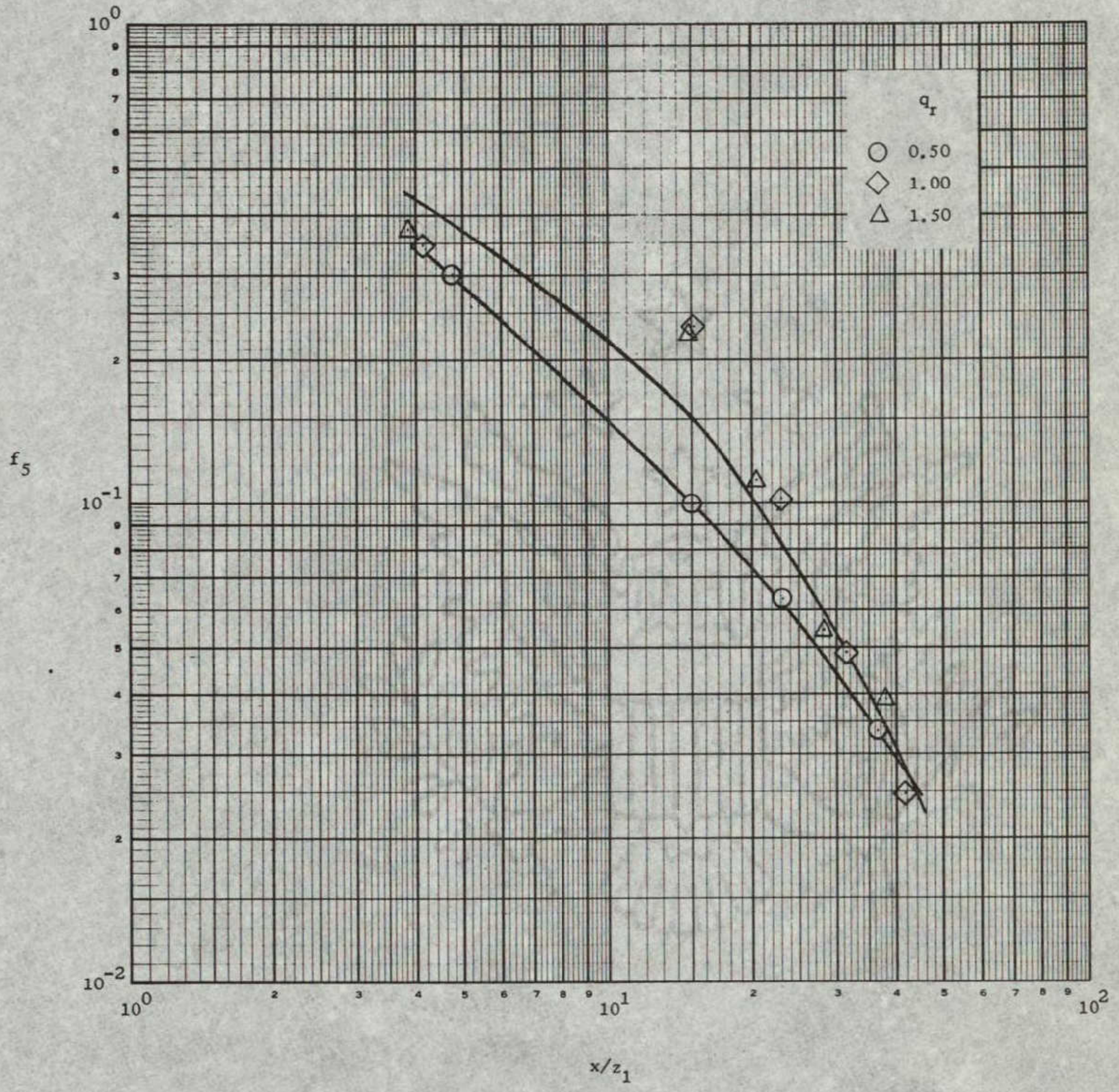

Figure 22.- Decay of average fuel-air ratio for simulated opposite wall injection.